HHS Public Access

Author manuscript

Neuroscience. Author manuscript; available in PMC 2020 February 01.

Published in final edited form as:

Neuroscience. 2019 February 01; 398: 126–143. doi:10.1016/j.neuroscience.2018.11.047.

Developmental changes in EEG phenotypes in a mouse model of Fragile X Syndrome

Teresa H. Wen[a], **Jonathan W. Lovelace**[b], **Iryna M. Ethell**[a,c], **Devin K. Binder**[a,c], and **Khaleel A. Razak**[a,b]

[a]Neuroscience Graduate Program, University of California Riverside, Riverside, California 92521, USA

[b]Psychology Department and Psychology Graduate Program, University of California Riverside, Riverside, California 92521, USA

[c]Division of Biomedical Sciences, School of Medicine, University of California Riverside, Riverside, California 92521, USA

Abstract

Fragile X Syndrome (FXS) is a leading genetic cause of autism and intellectual disabilities. Sensory processing deficits are common in humans with FXS and an animal model, the *Fmr1* knockout (KO) mouse, manifesting in the auditory system as debilitating hypersensitivity and abnormal electroencephalographic (EEG) and event-related potential (ERP) phenotypes. FXS is a neurodevelopmental disorder, but how EEG/ERP phenotypes change during development is unclear. Therefore, we characterized baseline and stimulus-evoked EEG in auditory and frontal cortex of developing (postnatal day (P) 21 and P30) and adult (P60) wildtype (WT) and *Fmr1* KO mice with the FVB genetic background. We found that baseline gamma-band power and N1 amplitude of auditory ERP were increased in frontal cortex of *Fmr1* KO mice during development and in adults. Baseline gamma power was increased in auditory cortex at P30. Genotype differences in stimulus-evoked gamma power were present in both cortical regions, but the direction and strength of the changes were age-dependent. These findings suggest that cortical deficits are present during early development and may contribute to sensory processing deficits in FXS, which in turn may lead to anxiety and delayed language. Developmental changes in EEG measures indicate that observations at a single time-point during development are not reflective of FXS disease progression and highlight the need to identify developmental trajectories and optimal windows for treatment.

Correspondence: Khaleel A. Razak, PhD, Department of Psychology, University of California Riverside, Riverside, California 92521, USA, Phone number: 951-827-5060, Facsimile number: 951-827-3985, khaleel@ucr.edu.

Conflict of Interest: The authors declare no competing financial interests.

Keywords

neurodevelopmental disorders; EEG; Fragile X Syndrome; gamma oscillations; sensory hypersensitivity

Fragile X Syndrome (FXS) is a leading inherited cause of autism and intellectual disability that affects 1 in 4000 males and 1 in 8000 females (O'Donnell and Warren, 2002). FXS occurs as a result of *Fmr1* gene hypermethylation, which leads to inactivation and loss of Fragile X Mental Retardation Protein (FMRP; Yu, et al., 1991). Symptoms of FXS include social and communication deficits, repetitive behaviors, sensory hypersensitivity, seizures and increased anxiety (Hagerman, et al., 1986; Baumgardner, et al., 1995; Harris, et al., 2008).

Abnormal auditory processing and hypersensitivity are documented in humans with FXS, through clinical observations (Miller, et al., 1999; Rogers, et al., 2003; Frankland, et al., 2004) and EEG recordings (Castrén, et al., 2003; Schneider et al., 2013; Ethridge et al., 2016; reviewed in Rotschafer and Razak, 2014 and Sinclair et al., 2016). The *Fmr1* KO mouse is a well-characterized pre-clinical model of FXS. Abnormal auditory processing and hypersensitivity are also evident in the mouse model of FXS. For example, audiogenic seizures and abnormal sensorimotor gating are consistently observed in *Fmr1* KO mice (Chen and Toth, 2001; Frankland et al., 2004). The similar hypersensitivity in humans with FXS and the mouse model increases the potential for translation relevant therapeutic approaches in FXS using sensory phenotypes as outcome measures (Rais et al., 2018). Additionally, sensory processing circuits may be relatively more conserved across species compared to those involving more complex cognitive and social behaviors.

Indeed, studies that examined electrophysiological responses using EEG recordings in adult/adolescent humans with FXS and adult *Fmr1* KO mice have found remarkably similar phenotypes. In both humans and mice, there is reduced habituation of N1 amplitude of auditory event related potentials in FXS (human: Castrén, et al., 2003; Van der Molen, et al., 2012a, Van der Molen, et al., 2012b; Schneider et al., 2013; Ethridge, et al., 2016, mouse: Lovelace, et al., 2016). Altered neural oscillatory activity is also revealed by baseline and sound-evoked EEG responses in both humans with FXS and the mouse model. Resting EEGs in humans with FXS showed reduced alpha (8–13 Hz) and increased theta (4–8 Hz) and gamma (30–80 Hz) power (Van der Molen, et al., 2013; Wang, et al., 2017). When neural oscillations are induced with oscillating stimuli, humans with FXS show reduced inter-trial phase coherence suggesting the inability to produce consistent trial-by-trial neural oscillations, particularly in the gamma band. The adult *Fmr1* KO mouse also shows increased baseline EEG gamma power and reduced inter-trial phase coherence to the same type of stimulus used in the human study (Sinclair et al., 2017; Lovelace et al., 2018). Single unit recordings show that *Fmr1* KO auditory cortical neurons are hyper-responsive, exhibit variable response latencies, and have broader tuning curves in response to tonal stimuli (Rotschafer and Razak 2013). In humans, the increased gamma-band activity during rest correlated negatively with performance on adult and adolescent sensory profiles (Wang, et al., 2017), indicating that altered network activity may be related to auditory hypersensitivity

phenotypes in FXS. Together, the similar EEG/ERP phenotypes in humans and mice related to FXS strongly suggest the use of these measures as biomarkers.

When phenotypes are characterized in adults with neurodevelopmental disorders, it is relatively difficult to disentangle direct effects of the genetic disorder from those that arise because of altered developmental experience. This can be partly addressed by examining the phenotypes during development to identify trajectories of change. Auditory cortex hyperexcitability and oscillation abnormalities in EEG may be attributed to altered development of GABAergic neurotransmission, particularly the development of parvalbumin (PV)-expressing neurons (Olmos-Serrano, et al., 2010; Wen, et al., 2017). Despite the prevalence of similar physiological abnormalities in humans with FXS and the mouse model, and known developmental changes in PV cell function, the developmental trajectory of EEG/ERP phenotypes in FXS remains unknown. Therefore, in this study, we characterized developmental changes in EEG/ERPs in the auditory and frontal cortex by recording these signals from postnatal day (P)21–24, P30–35, and adult *Fmr1* KO mice. We report that baseline and evoked EEG abnormalities are already present at P21 and that a number of phenotypes are either transient or show changes in direction and strength across the ages tested.

MATERIALS AND METHODS

Mice

Breeding pairs of FVB.129P2-Pde6b $^{+}$Tyr $^{c\text{-}ch}$ Fmr1^{tm1Cgr}/J (Jax 004624; *Fmr1* KO) and their congenic controls FVB.129P2-Pde6b $^{+}$Tyr $^{c\text{-}ch}$/AntJ controls (Jax 002848; WT) were obtained from the Jackson Laboratory and housed in an accredited vivarium on a 12-hour light/dark cycle. Food and water were provided *ad libitum* and confirmation of genotypes was conducted using PCR analysis of genomic DNA isolated from tail clippings. University of California, Riverside's Institutional Animal Care and Use Committee approved all procedures used. Experiments were conducted in accordance with NIH *Guide for the Care and Use of Laboratory Animals*. A total of 86 mice were used in this study (45 WT and 41 *Fmr1* KO mice).

We chose to study the FVB background here because previous studies have examined the development of parvalbumin expression, perineuronal nets and single unit responses in this strain (Rotschafer and Razak, 2013; Wen et al., 2017). *Fmr1* KO mice on FVB and C57Bl/6 backgrounds show differences in a number of neurobehavioral tests (Dobkin, et al., 2000; Nielsen, et al., 2002; Yan, et al., 2004; Spencer, et al., 2011; Reviewed in Kooy, et al., 2017), but whether electrophysiological measures are different remains unclear. In addition to novel developmental data, EEG recording from adult FVB mice provides the opportunity to compare with published EEG data from the adult C57/Bl6 mouse, which show robust differences between WT and *Fmr1* KO genotypes (Sinclair et al., 2017; Lovelace et al., 2018). Here we present new EEG data from 3 age groups of FVB strain mice. The FVB adult EEG data from this study can be compared to adult C57/Bl6 data from our previous study.

We recorded from both the frontal cortex (FC) and the auditory cortex (AC) in this study to compare with our previous work (Lovelace et al., 2018). The FC provides modulating input to the AC, and these connections are involved in top down control of auditory processing (Fritz, et al., 2010; Winkowski, et al., 2017). Indeed, simultaneous recordings of local field potentials in FC and AC show interesting patterns of change in the coherence between the two regions, which was related to behavior context. We established the method of recording from both AC and FC to conduct similar future experiments in mice performing specific trained behaviors. In the present study, we analyze the responses in these two cortical regions individually during development.

Surgery

Age-matched (P18–19, P28–30, and P45–80) WT and *Fmr1* KO animals were implanted with screw electrodes for EEG recordings. For the EEG screw implantation surgeries, mice were anesthetized with 80 mg/kg ketamine and 10 mg/kg xylazine, i.p. Dosage was halved for P18–19 mice, as these animals were more susceptible to overdose. Toe pinch reflex was monitored throughout and supplementary doses of ketamine/xylazine were given as needed. Once mice reached an areflexive state, a midline incision was made and the skull was exposed. A Foredom dental drill was used to drill three holes in right auditory cortex (−1.6 mm, +5.0 mm), left frontal cortex (+2.6 mm, −1.0 mm), and left occipital cortex (−3.5 mm, −5.2 mm) (coordinates relative to Bregma: anterior/posterior, medial/lateral). Three channel electrode posts (Plastics One, MS333–2-A-SPC) were attached to 1 mm stainless steel screws (Plastics One, 8L003905201F) and screws were advanced into three holes and secured with dental cement. Postoperative care included topical application of a triple antibiotic, and two subcutaneous injections of 0.1 mg/kg buprenorphine (0.05 mg/kg for P18–19 mice), one immediately after surgery and one 6–10 hours after surgery. After ambulation was restored, individually housed mice were returned to the vivarium and monitored daily until day of recordings. Mice were given between three to five days of post-operative recovery time and recordings were conducted in P21-P24 (WT N=15, KO N=15), P31–35 (WT N=17, KO N=16) and adult (P50–80) mice (WT N=13, KO N=10). These groups will be referred to as P21, P30 and P60 below. Of the mice studied, resting EEGs were obtained from 15 WT and 14 KO P21 mice; 17 WT and 16 KO P30 mice; and 13 WT and 10 KO P60 mice. ERPs were obtained from 15 WT and 15 KO P21 mice; 15 WT and 12 KO P30 mice; and 13 WT and 10 KO P60 mice.

Acoustic Stimulation

Sounds were generated using Real-Time Processor Visual Design Studio (RPvdsEx) software and delivered using RZ6 hardware (Tucker Davis Technologies, Alachua, FL). For auditory ERP recordings, a free-field speaker (MF-1 speakers, TDT, Alachua, FL) was mounted ~12 inches directly above a custom-made Faraday cage in which the mouse was placed. The sound levels of the stimuli were recorded with a ¼ inch Bruel and Kjaer microphone placed at the floor of the recording cage and adjusted to be presented at ~65–70 dB SPL (fluctuation of +/− 3 dB for frequencies between 5 and 35 kHz). We presented broadband noise trains (5–40 kHz, 100 ms duration) to record auditory ERPs in both genotypes across the three age groups. Each train consisted of 10 repetitions of broadband

noise presented at 0.25 Hz repetition rate, presented 100 times. Inter-train interval was 8 seconds. Each individual stimulus had a rise/fall time of 5 ms.

Electrophysiology

Mice were habituated for 20 minutes in an anechoic foam-lined soundproof chamber (Gretch-Ken Industries Inc.) and then placed inside the Faraday cage and connected to the BioPac acquisition system (BIOPAC Systems, Inc.) through a 3-channel tether threaded through the center of the Faraday cage. The tether was connected to a commutator located directly above the Faraday cage. Mice were habituated to being tethered to the commutator for an additional 20 minutes. ERPs evoked by broadband noise trains were then recorded. At the end of the recording, 5 minutes of resting EEG was recorded, and then mice were returned to the colony and perfused for histology at a later date. The BioPac MP150 acquisition system was connected to two EEG 100C amplifier units (one for each channel) to which the commutator was attached. The lead to the occipital cortex served as a reference electrode for the frontal and auditory cortex screws. Acquisition hardware was set to high-pass (>0.5 Hz) and low-pass (<100 Hz) filters. Acqknowledge recording software was used to record EEG activity while mice were awake and freely moving. Data were sampled at a rate of either 2.5 or 5 kHz via Acqknowledge software and then down-sampled to 1024 Hz using Analyzer 2.1 (BrainVision Inc.).

Data Analysis

EEG traces were extracted from Acqknowledge and converted to files compatible with Analyzer 2.1. EEG data was notch filtered at 60 Hz to remove residual line noise from recordings. Artifact rejection was performed semi-automatically using Brain Vision Analyzer. Several criteria were used to search for artifacts including amplitude, gradient, max-min and low activity. Low activity was almost always due to padding zeroes at the end of the data to account for sampling rate. 99% of artifacts were detected due to large amplitude fluctuations (set absolute threshold). Gradient and max-min were less likely to be detected.

Resting EEG analysis: Five minutes of EEG traces were divided into segments of 1 sec length, and Fast Fourier Transform (FFT, 0.5 Hz resolution) was calculated. From the FFT data, average absolute power ($\mu V/Hz^2$) in each for the following frequency bands was computed for each mouse: Delta 1–4 Hz, Theta 4–8 Hz, Alpha 8–13 Hz, Beta 13–30 Hz, Gamma 30–100 Hz (55–64 Hz was omitted to account for 60 Hz notch). Recent studies suggest that gamma rhythms in the 30–60 Hz band and higher frequency broadband gamma (>50 Hz) are distinct and generated by different mechanisms (Dvorak and Fenton, 2014; Balakrishnan and Pearce 2015). The lower gamma frequency rhythm may be associated with activity of parvalbumin cells while the higher gamma frequencies may be related to spiking activity near the electrodes (Ray and Maunsell 2011; Buzsáki and Wang 2012). To determine if there were additional differences in the low and high gamma frequency bands in our recordings, gamma was further divided into low (30–54 Hz) and high gamma frequency bands (64–100 Hz). The spectral bands used are based on a number of previous studies on FXS in both mice (e.g., Radwan et al., 2016) and humans (Ethridge et al., 2016, Wang et al., 2017). The utility of analyzing spectral bands is related to data that show that different

circuit elements and computations may underlie distinct bands (Kuki et al., 2015; Chen et al., 2017) and changes in the power at different bands are related to specific aspects of cognition.

As movement can alter cortical gain (Niell and Stryker 2010), a piezoelectric transducer was placed under the EEG recording arena to quantify movement in P21 (WT N=15, KO N=14) and P30 (WT N=15, KO N=11) animals. The first dataset was collected in adult mice, and we did not record movement data in these mice. A threshold criterion was established for detection of movement using the signal from the piezoelectric transducer and confirmed with video recordings taken during the entire duration of the EEG recording. To conform to assumptions necessary for ANOVA, including normality and homogeneity of variance, a log transform was applied to resting EEG data and a rank-based Blom transform was applied to ERP data when violations of assumptions were detected. Two-way ANOVA (genotype-WT vs. KO × frequency band-delta, theta, alpha, beta, gamma) was used to test for genotype differences at specific ages. When gamma was split into low and high gamma, the frequency factor consisted of six levels (delta, theta, alpha, beta, low gamma, high gamma). To test for effects of movement on differences in resting gamma (low/high), movement was converted into a binary value (move or still) and a three-way ANOVA was used (genotype × frequency band × movement). In all cases, p values < 0.05 were considered significant. When interactions were found and multiple comparisons for ANOVA were made, data were analyzed on each factor for simple effects and corrected for using Bonferroni adjustments. Post-hoc analyses were only conducted for age and for genotype. For age, three comparisons were made (P21 vs. P30, P30 vs. P60, P21 vs. P60), so p-values were adjusted using a divisor of 3.

ERP analysis: After artifact rejection, EEG trains were divided into 4-second segments based on a TTL pulse that marked the onset of the sound stimulus. A grand average ERP was obtained from all stimulus-evoked responses. P1, N1, and P2 were identified based on maximal positive or negative deflections in specific time windows: P1 (10–30 ms), N1 (30–80 ms), and P2 (80–150 ms). For characterization of developmental differences in each genotype, a two-way ANOVA was used (age × frequency band). In all cases, p <0.05 were considered significant. When interactions were found and multiple comparisons for ANOVA were made, data were analyzed on each factor for simple effects and corrected for using Bonferroni adjustments.

In addition to ERP peak amplitude and latency analysis, stimulus-evoked responses were segmented into windows of 200 ms before BBN onset to 700 ms after stimulus onset. The initial 200 ms prestimulus window was used to calculate baseline corrected evoked non-phase locked power from 0 to 700 ms after stimulus onset. Power density (μV^2/Hz) was characterized using Morlet wavelets from 1–100 Hz with 1 Hz steps and wavelet parameter of 10. A custom Matlab script was used to compare stimulus-evoked power in WT and *Fmr1* KO mice. Analysis was conducted by binning time into 225 parts and frequency into 100 parts, resulting in a 100×225 matrix. Non-parametric cluster analysis was used to determine whether contiguous spatiotemporal matrix regions were significantly different from a distribution of 1000 randomized Monte Carlo permutations (Maris and Oostenveld, 2007). If the cluster sizes of the real genotype assignments were larger than 97.25% of the randomly

assigned groups, clusters were considered significant (two-tailed alpha of p=0.025). This method was used to correct for multiple comparisons, and avoids statistical assumptions about the data.

RESULTS

Resting EEG and auditory ERP from two cortical regions (auditory and frontal cortex: henceforth, AC and FC, respectively) were examined at three different ages (P21-P24, P31-P35 and young adults: henceforth, P21, P30 and P60, respectively) and in two genotypes (WT and *Fmr1* KO mice) to determine baseline and sound-evoked neural responses. As previous studies indicate cortical hyperexcitability and reduced perineuronal net expression around inhibitory interneurons at P21 (Wen et al., 2017), we hypothesized that EEGs recorded at this age would exhibit altered gamma-band activity. P30 was chosen as a second developmental time point for two main reasons. First, the mouse auditory cortex is not fully mature until P30 in terms of response selectivity to complex sounds (Carrasco et al., 2013). Second, a number of phenotypes in FXS model mice show developmental fluctuations (reviewed in Meredith et al., 2012). In particular, both sound evoked auditory cortex response magnitude and dendritic spine densities are relatively normal ~P30, although they are abnormal at younger and older ages. Therefore, we examined EEGs at P30 as well. Broadband noise-evoked event related potentials (ERP) were recorded to determine whether increased cortical N1 amplitudes detected in adult *Fmr1* KO mice (Lovelace et al., 2018) are also observed in development. We first present the analysis of developmental EEG changes in FC and AC of WT and KO mice separately, and then compare the two genotypes. The WT mouse data would be broadly useful across pre-clinical studies of neurodevelopmental disorders.

Region-specific developmental changes in absolute resting EEG power in WT and *Fmr1* KO mice

Figure 1 shows samples of resting EEG recordings obtained from the AC and FC of WT and *Fmr1* KO mice at P21 and P30 (Fig. 1). We quantified absolute EEG spectral power in AC of normally developing WT mice at P21, P30, and P60 in the baseline (no stimulus) condition (Fig. 2A1, A2). There was an effect of frequency: $F(5,252)=363.620$, $p<0.0001$, and an effect of age $F(2,252) = 4.570$, $p<0.05$, but no significant interactions in the AC with a two-way ANOVA (age × frequency). This indicates that absolute power varied across frequency bands as expected (‘1/f’ EEG power profile). In addition, there was a general increase in power from P21 to P30 (Bonferroni test of main effects, P21 vs. P30 $p<0.05$) in AC of WT mice. Power was not different between P30 and P60 (Bonferroni test of main effects, P30 vs. P60 $p>0.05$). This suggests that the circuits generating baseline neural oscillations at various frequencies in the auditory cortex become adult-like between P21 and P30.

Analysis of baseline EEG recordings in FC of WT mice revealed an effect of age and frequency (Fig. 2B1, B2): age $F(2,252)=41.879$, $p<0.0001$; frequency $F(5,252)=757.617$, $p<0.0001$. The FC exhibited a developmental increase in overall absolute power across frequency bands (Bonferroni test of main effects, P21 vs. P30 $p<0.0001$, P21 vs. P60

p<0.0001; P30 vs. P60 p<0.0001). There was also a significant age × frequency interaction: F(10,252)=2.769, p<0.01, indicating that specific frequency bands exhibited larger developmental changes in absolute power. This was particularly evident in the low frequencies (delta and theta bands) in which absolute power increased between P21 and P60 (Bonferroni multiple comparisons post-test, delta: P21 vs. P30 p<0.05, P30 vs. P60 p<0.0001, P21 vs. P60 p<0.0001; theta: P30 vs. P60 p<0.01; P21 vs. P60 p<0.0001). Age-related increases in absolute power were also evident in the alpha (P21 vs. P60 p<0.01) and high gamma frequency bands (P30 vs. P60 p<0.05; P21 vs. P60 p<0.001).

Developmental changes in absolute EEG spectral power in *Fmr1* KO mice (Fig. 3) exhibited similar trends to those in WT mice. In AC of *Fmr1* KO mice, we observed an effect of frequency: F(5,222)=272.458, p<0.0001, and age: F(2,222)=3.293, p<0.05, but no interactions (Fig. 3A1, A2). The main effect of age was attributed to an increase in EEG power from P21 to P30 (Bonferroni test of main effects, P21 vs. P30 p<0.05). In FC of KO mice, there were main effects of frequency: F(5,222)=476.087, p<0.0001 and age: F(2,222)=63.598, p<0.0001 indicating that FC of KO mice also exhibits a developmental increase in absolute power (Fig. 3B1, B2; Bonferroni test of main effects, P21 vs. P30 p<0.0001, P30 vs. P60 p<0.0001, P21 vs. P60 p<0.0001). Moreover, there was a significant age × frequency interaction: F(10,222)=4.360, p<0.0001, which was driven by age-related changes in absolute power across almost all frequency bands (Bonferroni multiple comparisons post-test, delta: P21 vs. P30 p<0.0001, P30 vs. P60 p<0.001, P21 vs. P60 p<0.0001; theta: P21 vs. P30 p<0.01, P30 vs. P60 p<0.01, P21 vs. P60 p<0.0001; alpha: P21 vs. P60 p<0.001; beta: P21 vs. P60 p<0.05; high gamma: P30 vs. P60 p<0.01; P21 vs. P60 p<0.0001). These data suggest that in both genotypes, the generators of neural oscillations in the FC continue to mature well into young adulthood. In the AC, responses reach maturity between P21 and P30, as suggested based on single unit recordings of response selectivity (Carrasco et al., 2013).

Increased gamma band power is seen as early as P21 in *Fmr1* KO mice

Increased gamma power has been observed in adult *Fmr1* KO mice in both AC and FC (Lovelace et al., 2018). In order to determine whether similar genotype-specific differences in spectral power are present in developing *Fmr1* KO AC and FC, we compared resting EEG power at P21, P30 and P60 between WT and *Fmr1* KO mice. Absolute power in each frequency band was divided by the corresponding absolute power in WT mice and presented as a ratio of WT (Fig. 4, 6, 8). A ratio greater than 1 indicates increased power in KO compared to WT.

In the AC, normalized resting EEG power across all frequency bands was comparable between *Fmr1* KO and WT mice at P21 (Fig. 4A1–A3). In the FC (Fig. 4B1–B3), there was an effect of frequency and a trend for an effect of genotype (genotype F(1,135)=3.579, *p=0.061*; frequency F(4,135)=2.929, p<0.05). This was likely due to increased gamma band power in *Fmr1* KO mouse, as analysis of both low (30–54 Hz) and high gamma (64–100 Hz) frequency bands indicated a main effect of genotype: F(1,54)=7.728, p<0.01 (Fig. 4B3). These data indicate increased gamma band baseline EEG power in *Fmr1* KO mice in FC, but not AC, at P21.

As movement can modulate cortical activity (Niell and Stryker, 2010) and because *Fmr1* KO mice are hyperactive (Spencer, et al., 2005), we characterized movement-related changes in resting gamma power. Although P21 WT and *Fmr1* KO mice spent a similar amount of time moving (Fig. 5A; independent samples t-test, $p>0.05$), we characterized power in low and high gamma frequency bands during periods of non-movement (Fig. 5B1) and periods of movement (Fig. 5B2). A three-way ANOVA was conducted to probe for interactions of movement, genotype, and frequency. A main effect of genotype, but not movement or frequency, was observed, indicating that *Fmr1* KO mice exhibited increased power in low and high gamma frequency bands independent of movement (three-way ANOVA: genotype $F(1,102)=27.393$, $p<0.0001$; movement, $p>0.05$; frequency/low vs. high gamma, $p>0.05$; all interactions, $p>0.05$). An additional two-way ANCOVA analysis was conducted with movement as a covariate. While movement accounted for ~40% of the variance, an effect of genotype was still observed (twoway ANCOVA: genotype $F(1,53)=14.988$, $p<0.001$; frequency/low vs. high gamma, $p>0.05$; covariate/movement $F(1,53)=38.392$, $p<0.0001$; genotype × frequency/low vs. high gamma, $p<0.05$). Thus, increased gamma power in the FC of P21 *Fmr1* KO mice as compared to WT mice was independent of any movement-related changes in gamma band activity.

Increased gamma band power in both AC and FC in P30 *Fmr1* KO mice

At P30, both AC and FC of *Fmr1* KO mice showed enhanced gamma power. In the AC, a significant, main effect of genotype on gamma-band power was observed when low and high frequency gamma were evaluated (Fig. 6A1–A3; two-way ANOVA: genotype $F(1,62)=5.510$, $p<0.05$; frequency/low vs. high gamma, $p>0.05$; genotype × frequency/low vs. high, $p>0.05$). Increased gamma-band power was also observed in FC of *Fmr1* KO mice (Fig. 6B1–B3; two-way ANOVA: genotype $F(1,62)=5.29$, $p<0.05$; frequency/low vs. high gamma, $p>0.05$; genotype × frequency/low vs. high gamma, $p>0.05$).

As both AC and FC exhibited increased gamma power in *Fmr1* KO mice at P30, we again characterized the effects of movement on gamma power. At P30, WT and *Fmr1* KO mice also spent a comparable amount of time moving (Fig. 7A; independent samples t-test, $p>0.05$). In both KO AC (Fig. 7B1, B2) and KO FC (Fig. 7C1, C2), gamma power was enhanced in gamma frequency bands, independent of movement (three-way ANOVA auditory cortex: genotype $F(1,94)=12.017$, $p<0.001$; movement $p>0.05$; frequency/low vs. high gamma $p>0.05$; all interactions $p>0.05$; frontal cortex: genotype $F(1,94)=8.892$, $p<0.01$; movement $p>0.05$; frequency/low vs. high gamma, $p>0.05$; all interactions, $p>0.05$). When movement was included as a covariate in a two-way ANCOVA, similar results were observed (two-way ANCOVA auditory cortex: genotype $F(1,47)=7.820$, $p<0.01$; frequency/low vs. high gamma, $p>0.05$; covariate/movement $F(1,47)=17.514$, $p<0.001$; genotype × frequency/low vs. high gamma, $p<0.05$; frontal cortex: genotype $F(1,47)=4.134$, $p<0.05$; frequency/low vs. high gamma, $p>0.05$; covariate/movement $F(1,47)=24.532$, $p<0.0001$; genotype × frequency/low vs. high gamma, $p<0.05$). These results indicate that increased gamma power observed in AC and FC of P30 *Fmr1* KO mice is independent of movement-related changes in gamma.

Increased gamma band power only in FC of young adult *Fmr1* KO mice

Similar to P21, baseline EEG power across all frequency bands in AC of P60 *Fmr1* KO mice was comparable to P60 WT (Fig. 8A1–A3; two-way ANOVA: genotype $p>0.05$; frequency $p>0.05$; genotype × frequency, $p>0.05$). In contrast, gamma power was enhanced in FC of P60 KO mice (Fig. 8B1–B3; two-way ANOVA: genotype $F(1,42)=5.259$, $p<0.05$; frequency/low vs. high gamma, $p>0.05$; genotype × frequency/low vs. high gamma, $p>0.05$), similar to P21 and P30 *Fmr1* KO mice. Movement data were not recorded for the adult mice, and therefore movement-related analyses were not conducted. In summary, these results indicate that enhanced gamma power in the *Fmr1* KO mouse FC is observed both in developing and adult *Fmr1* KO mice. Genotype differences in gamma power in the AC were only observed at P30.

Developmental changes in auditory ERP in WT and *Fmr1* KO cortex

To determine whether the developing *Fmr1* KO mice show altered ERP latency and amplitude, we measured ERPs to a 100 ms broadband noise stimulus. The grand average ERP waveforms were plotted for WT and *Fmr1* KO mice at P21 (Fig. 9A1, B1), P30 (Fig. 9A2, B2), and P60 (Fig. 9A3, B3). Peak amplitude and peak latency were measured from individual animal average waveforms and resultant grand average amplitude (Fig. 9C1–C3, D1–D3) and latency (Fig. 10) were used to characterize genotype and age effects.

For N1 amplitude, there was a significant, main effect of age in both AC (Fig. 9C2; twoway ANOVA: age $F(2,74)=10.858$, $p<0.0001$; genotype, $p>0.05$) and FC (Fig. 9D2; two-way ANOVA: age $F(2,74)=4.102$, $p<0.05$; genotype $F(1,74)=11.989$, $p<0.001$), indicating that N1 amplitude increases with age (N1 becomes more negative) (Bonferroni test of main effects, auditory cortex: P21 vs. P60 $p<0.0001$, P30 vs. P60 $p<0.05$; frontal cortex: P21 vs. P60 $p<0.05$). A main effect of genotype was also observed, but only in FC, suggesting that N1 amplitude is larger in FC of *Fmr1* KO compared to WT throughout development. There were no age- or genotype-related changes in either P1 or P2 amplitude (Fig 9C1, D1, C3, D3).

Developmental changes in ERP latency were not observed in AC of WT or *Fmr1* KO mice. In the FC, however, N1 latency decreased with age (Fig. 10B2; two-way ANOVA: age $F(2,74)=3.256$, $p<0.05$; Bonferroni test of main effects, P30 vs. P60 $p<0.05$). The N1 latency was longer in the AC of *Fmr1* KO mice at P60 (Fig. 10A2; genotype × age $F(2,70)=3.305$, $p<0.05$; P60 WT vs. KO $p<0.05$). Genotype differences were not observed for P1 or P2. In summary, N1 amplitude in FC was larger across age groups in *Fmr1* KO mice compared to WT. N1 latency was longer in the KO at P60 and latencies of the N1 component decreased with age in the FC across both genotypes.

As non-phase locked power during auditory stimulus presentation is increased in humans with FXS (Ethridge, et al., 2016), we determined whether a similar phenotype is observed developmentally in *Fmr1* KO mice by quantifying responses to broadband noise (Fig. 11). In the AC of P21 *Fmr1* KO mice, increased non-phase locked power was most robust in the gamma frequency band following stimulus presentation (Fig. 11A1, A4). However, at P30, non-phase locked gamma power was significantly reduced in *Fmr1* KO mice compared to

WT mice (Fig. 11A2, A5). In adult AC, non-phase locked power was comparable between WT and KO mice (Fig. 11A3, A6) similar to the data from adult C57/Bl6 mice Sinclair et al., 2017).

Developmental changes in the direction and strength of genotype differences in non-phase locked gamma power were also observed in FC. Gamma-band power was increased in FC of P21 *Fmr1* KO mice following stimulus onset (Fig. 11B1, B4). In contrast, gamma power was reduced in FC of P30 *Fmr1* KO mice as seen in the AC (Fig. 11B2, B5). Interestingly, unlike AC, adult FC in *Fmr1* KO mice exhibited a rather robust increase in gamma frequency power (Fig. 11B3, B6). The increase in non-phase locked gamma power in adult FC of *Fmr1* KO mice continued well after stimulus offset. Together, the EEG/ERP analyses revealed complex and spatially (AC *vs.* FC) distinct developmental trajectories of EEG/ERP phenotypes in the *Fmr1* KO mice.

DISCUSSION

This study identified region (AC and FC), genotype (WT and *Fmr1* KO mice) and age (P21, P30 and P60) specific differences in resting cortical oscillatory activity and stimulus-evoked responses. Resting gamma power was elevated in FC of *Fmr1* KO mice at P21, P30, and P60, whereas AC showed an increase in resting gamma power only at P30. Larger N1 amplitude was observed across development in FC of *Fmr1* KO mice, but no genotype differences were present in the AC. Genotype differences in stimulus-evoked non-phase locked gamma power varied both developmentally and spatially. In the AC, stimulus-evoked gamma power was enhanced in the KO mouse at P21, was significantly reduced at P30 and showed no genotype difference at P60. In FC, stimulus-evoked gamma power was increased at P21 and P60, but was reduced at P30 in KO mice compared to WT mice. These data indicate that considerable physiological differences are already detectable at P21 in *Fmr1* KO mice. Auditory hypersensitivity seen in adults and adolescents with FXS may be driven by abnormal cortical responses and network oscillatory activity during development. Observations made about a FXS phenotype at a single time point may not accurately reflect the dynamic changes and the potential compensatory mechanisms that may be recruited in the face of reduced FMRP in FXS brain development. To better understand the pathophysiology of FXS, these results argue for increased characterization of developmental trajectories of FMRP-related functions and FXS-associated phenotypes (Berry-Kravis et al., 2018; Hoeft et al., 2010).

Maturation of EEG/ERP responses in auditory and frontal cortex of mice

The WT mouse data provide insights into normal age-specific changes in EEG/ERP characteristics in AC and FC of mice. The baseline EEG profile in the auditory cortex is adult-like by at least P30. The timeline for EEG maturation in other sensory cortices varies. In mouse visual cortex, the baseline power spectral density profile is largely mature by P12–14 (Shen and Colonnese, 2016). Developmental EEG data from rat somatosensory cortex (Devonshire et al., 2015; Chang et al., 2016) indicates maturation at or around P21. These results lead to the conclusion that sensory cortical generators of baseline neural oscillations are largely mature at or before P30. However, adult-like pattern of spectral power in baseline

EEG, particularly in low frequency bands (delta, theta), matured more slowly in the frontal cortex. Compared to baseline EEG, auditory ERP amplitudes and latencies showed similar developmental patterns in both AC and FC. ERP N1 amplitudes, but not P1 or P2 amplitudes, increased with age in both AC and FC, and N1 latency decreased with age in FC.

The developmental increase in N1 amplitude (more negative) in WT mice is similar to that observed in humans (Ponton et al., 2000; Ponton, et al., 2002) and in other rodent studies (Iwasa and Potsic, 1982; Shen and Colonnese, 2016). An age-related decrease in N1 latency was observed in the present study, and this is also similar to previous studies (Ponton et al., 2000; Ponton, et al., 2002; Iwasa and Potsic, 1982; Shen and Colonnese, 2016). However, P1 and P2 latencies were mature at P21 in both regions in the mouse. The relatively modest changes in ERP latencies in WT mice are in contrast to those observed in humans (Ponton et al., 2000; Ponton, et al., 2002), reflecting likely species differences in development of myelination. In summary, the mouse baseline EEG data suggests slower maturation of neural oscillations in FC compared to AC, consistent with anatomical markers of cortical maturation (Gogtay, et al., 2004; Deoni, et al., 2015; Sowell et al., 1999). In terms of ERP amplitude and latency, both AC and FC show similar trajectories of maturation.

Development of genotype differences in baseline EEG and auditory ERP

Developmental changes in genotype differences in EEG/ERP measures were observed (e.g., Fig. 11). Some of the changes were seen only transiently (e.g., P30 AC resting gamma increase). The non-phase locked sound evoked gamma power was robustly increased in both AC and FC of the KO mouse at P21. However, by P30, these differences were reversed in direction. In adults, there was no genotype difference in AC, but the power was robustly enhanced in KO FC. An intriguing aspect of adult *Fmr1* KO FC data is that such increased power was sustained well after the sound offset and showed periodicities reminiscent of data reported in rat visual cortex around eye opening (Colonnese et al., 2010). The mechanisms underlying the slow modulations of such long duration responses remain unclear in the adult *Fmr1* KO FC, but future studies on cross-frequency coupling of EEG signals within and across areas will provide insights (Radwan et al., 2016).

Such developmental fluctuations and transient changes in cellular and physiological phenotypes appear to be the rule rather than the exception in FXS (reviewed in Meredith et al., 2012; Meredith 2015). For instance, altered synaptic connectivity and spine morphology in *Fmr1* KO mouse somatosensory cortex only appear transiently during development. In the hippocampus, spine length is increased at P10, decreased at P30 and normal at P40 in KO compared to WT mice. Neural connectivity patterns in KO frontal cortex are abnormal between P12–21, but normal in adults. Single unit responses to sounds are increased in the auditory cortex of *Fmr1* KO mice at P21 and adults, but not at P14 and P30 (Rotschafer and Razak, 2013; Wen et al., 2017). In visual cortex of *Fmr1* KO rats, there is evidence for hypo-excitability before eye-opening (P8–11), followed by normal development of visual responses, and then later onset of neuronal hyperexcitability by P19–24 (Berzhanskaya, et al., 2016). Transient changes that occur during critical developmental plasticity windows (Dölen et al., 2007; Kim et al., 2013) can induce compensatory mechanisms that can be

abnormally stabilized into adulthood. Therefore, the outcomes measured at different ages are likely a result of both direct effect of the genetic mutation and the effects of the system compensating (e.g., homeostatic plasticity) for abnormal input patterns and processing. Future studies that delete or re-express FMRP at specific time points (Siegel, et al., 2017) are needed to determine how the absence of FMRP influences disease progression at various time points. It is also critical to study the developmental changes in FMRP levels and target proteins in the auditory cortex to reveal putative relationships between specific molecular pathways and physiological outputs. These studies have considerable implications in terms of optimal treatment windows in clinical trials and utility of potential gene reactivation in adults (Liu, et al., 2018).

Mouse background strain differences in EEG/ERP phenotypes

Together with published work, this study facilitates a comparison of background strain effects on EEG phenotypes in adult *Fmr1* KO mice (C57Bl6 versus FVB, summarized in Table 1). Specifically, adult *Fmr1* KO mice on the C57Bl6 background show robust deficits in gamma power in both the AC and FC (Lovelace, et al., 2018). However, enhanced baseline gamma power was observed only in the FC of the adult FVB KO mice. The C57Bl6 and FVB mice were similar in terms of enhanced N1 amplitudes in the FC. Neither strain showed a significant difference in N1 amplitude in the AC. The lack of a genotype difference in non-phase locked gamma power in adult AC is similar in FVB mice (this study) and the C57Bl6 mice (Sinclair et al., 2017). Strain differences in behavioral phenotypes have been reported in *Fmr1* KO mice on the C57Bl6 *vs*. FVB backgrounds (Dobkin, et al., 2000; Nielsen, et al., 2002; Yan, et al., 2004; Spencer, et al., 2011; Reviewed in Kooy, et al., 2017). An extensive study by Spencer and colleagues comparing the effect of *Fmr1* KO in C57Bl6 and a number of F1 hybrid lines demonstrated that congenic C57Bl6 *Fmr1* KO mice exhibited anxiety-like phenotypes and impaired sociability, as measured by performance in a light-dark box and social interaction tests (Spencer, et al., 2011). Interestingly, these behaviors appeared normal in C57Bl6/FVB hybrid *Fmr1* KO mice. Congenic C57Bl6 KO mice also exhibit reduced prepulse inhibition, which is normal in C57Bl6/FVB hybrid *Fmr1* KO mice (Nielsen, et al., 2002). While these findings may indicate attenuated behavioral phenotypes in FVB KO mice, other studies indicate that *Fmr1* KO mice on the FVB background exhibit impaired cross water maze learning, which is not impaired in C57Bl6 KO mice (Dobkin, et al., 2000). Comparison of acoustic startle responses indicates that both C57Bl6 KO and FVB KO mice have decreased startle responses at particularly loud startle intensities compared to WT, mice, while startle responses in C57/Bl6/FVB hybrid KOs are not different from hybrid controls (Chen and Toth 2001; Nielsen, et al., 2002; Frankland, et al., 2004). Both strains are susceptible to audiogenic seizures (Yan, et al., 2004). Whether the EEG phenotypes observed in FVB and C57 *Fmr1* KO mice may be utilized to predict severity of specific behavioral phenotypes remains to be studied. However, strain differences in phenotypes could potentially be used to model stratification of human population according to EEG patterns and identify differential sensitivity to various therapeutic options.

Methodological issues

The WT and *Fmr1* KO mice compared in this study were not littermates, and therefore an important caveat is that the findings presented may be attributed to either loss of the *Fmr1* gene or indirect effects such as differences in maternal care. We have conducted littermate studies in the adult C57/Bl6 mice recently (Lovelace et al., in preparation) and compared to our previous adult C57/Bl6 data (Lovelace et al., 2018), which did not use littermates. The results were essentially identical strongly suggesting the phenotypes observed are a result of the *Fmr1* knock out, and not due to potentially different maternal effects. The gamma deficits we report are consistent across multiple studies regardless of whether (Boone et al., 2018; Dasilva et al., 2018) or not littermate (Sinclair et al., 2017, our studies) controls were used.

Functional implications and potential mechanisms

The larger ERP N1 amplitudes and non-phase locked sound-evoked power seen in FXS adults and adolescents (Castrén, et al., 2003; Van de Molen, et al., 2012a; Schneider, et al., 2013; Ethridge, et al., 2016) are also observed in *Fmr1* KO mice across development (this study). ERP development in FXS patients has not been studied. Enhanced stimulus-evoked response magnitudes and increased neural synchrony have been previously characterized in cortex of both developing and adult *Fmr1* KO mice (Gibson, et al., 2008; Gonçalves, et al., 2013, Arnett, et al., 2014; Zhang, et al., 2014; Lovelace, et al., 2016; Wen, et al., 2017). These findings, in conjunction with increased resting gamma and spontaneous UP states, indicate that a greater number of neurons in *Fmr1* KO mice fire synchronously to sensory stimuli (Reviewed in Contractor, et al., 2015). For example, in mature KO somatosensory cortex, a larger cortical area is activated when whiskers are stimulated (Arnett, et al., 2014; Zhang, et al., 2014). In the mature KO auditory cortex, neurons show broader frequency tuning curves (Rotschafer and Razak 2013). This would cause more neurons to be activated synchronously for any single sound generating larger evoked responses.

Altered baseline and evoked gamma power were observed during development in the AC. The aberrant gamma responses in the EEG signals may reflect abnormal development and function of parvalbumin (PV)-expressing GABAergic interneurons in the *Fmr1* KO mouse cortex. PV neurons play a pivotal role in the generation of gamma oscillations (Sohal, et al., 2009; Chen, et al., 2017). In the somatosensory cortex of *Fmr1* KO mice, the excitatory drive to PV neurons is reduced, thereby reducing circuit level inhibition (Gibson, et al., 2008). PV neuron development is delayed in both AC and somatosensory cortex (Wen, et al., 2017; Nomura, et al., 2017). In the AC, there is a reduction of perineuronal net expression around PV neurons at P21 (Wen, et al., 2017). Because PV neuron excitability is reduced when PNN is absent (Balmer, et al., 2009; Lensjø, et al., 2017), this delay will also lead to reduction of inhibition in the cortical microcircuit. The loss of PNN was linked to increased activity of matrix-metalloproteinase-9 (MMP-9), an endopeptidase that cleaves extracellular matrix components. MMP-9 is an FMRP translational target and is elevated throughout development in the auditory cortex of *Fmr1* KO mice (Janusz, et al., 2013; Wen, et al., 2017). These data together strongly argue that the hyperexcitability revealed by electrophysiological recordings in the AC may be due to reduced inhibition mediated through PV-expressing interneurons.

Increased resting gamma is a robust EEG phenotype, evident in both developing and adult *Fmr1* KO mice, across mouse strains (C57Bl6 and FVB) and is also observed in humans with FXS (Wang, et al., 2017). Increased gamma power has also been observed in the *Fmr1* KO rat model (Berzhanskaya, et al., 2017). Studies in visual processing and perceptual organization suggest that the highly synchronous network activity which drives gamma oscillations contributes to 'temporal binding', which enables local cortical networks encoding different features to be combined in order to form perception of the entire object (Reviewed in Brock, et al., 2002; Reviewed in Jensen, et al., 2007). If baseline gamma is already high, elevated levels of synchronous firing would contribute to increased excitatory drive in the cortex, resulting in modulation of gain, neuronal hyperexcitability, and larger stimulus-evoked N1 (Reviewed in Jensen, et al., 2007), which may disrupt normal perceptual organization and lead to sensory hypersensitivity in FXS (Kogan, et al., 2004a, Kogan, et al., 2004b; Rogers, et al., 2003; Reviewed in Bertone, et al., 2010). Additionally, because levels of attention are correlated with gamma power (Bauer, et al., 2006; Gregoriou, et al., 2009), altered gamma oscillations may underlie impaired attention and executive function in FXS (Cornish, et al., 2004). Whether these cortical EEG phenotypes are sufficient to evaluate perceptual, attention, and language deficits in FXS remains to be tested. However, recent studies in humans and rodents have demonstrated that the magnitude of cortical EEG deficits correlates with severity of behavioral abnormalities, including social and communication deficits and sensory hypersensitivity (Wang, et al., 2017; Sinclair, et al., 2017). These significant correlations between behaviorally relevant phenotypes in FXS patients and specific EEG deficits strongly support the feasibility of defining EEG biomarkers that will be useful for evaluating the efficacy of interventional strategies in FXS.

In conclusion, this study reveals multiple EEG alterations in the cortex of developing *Fmr1* KO mice. The presence of abnormal EEG signals as early as P21 suggests that correction of FXS phenotypes will need to be done earlier in development to prevent cortical circuit maturation abnormalities. Indeed, drug treatments in young *Fmr1* KO mice have long-lasting benefits for anxiolytic behavior (Dansie, et al., 2013) and immature dendritic spines (Su, et al., 2011) in rodents. Future experiments, which test the therapeutic efficacy of treatments during early development on EEG/ERP measures in adults, will determine whether long-term benefits arise. Studies that examine effects of deleting FMRP at specific developmental windows are also critical.

Acknowledgements:

We thank the members of the Ethell, Binder and Razak labs for critical discussions that led to the ideas developed in this manuscript.

Funding: This work was supported by an NIH center grant for collaborative research in FXS (1U54 HD082008–01 to I.M.E., D.K.B., and K.A.R.) and an U.S. Army Medical Research and Materiel Command (W81XWH-15–1–0436 to I.M.E., D.K.B., and K.A.R.).

References

Arnett MT, Herman DH, McGee AW 2014 Deficits in tactile learning in a mouse model of fragile X syndrome. PloS One. 9(10): e109116. [PubMed: 25296296]

Balakrishnan S and Pearce RA, 2015 Spatiotemporal characteristics and pharmacological modulation of multiple gamma oscillations in the CA1 region of the hippocampus. Frontiers in Neural Circuits. 8: 150. [PubMed: 25628540]

Balmer TS, Carels VM, Frisch JL, Nick TA 2009 Modulation of perineuronal nets and parvalbumin with developmental song learning. Journal of Neuroscience. 29(41): 12878–12885. [PubMed: 19828802]

Bauer M, Oostenveld R, Peeters M, Fries P 2006 Tactile spatial attention enhances gamma-band activity in somatosensory cortex and reduces low-frequency activity in parieto-occipital areas. Journal of Neuroscience. 26(2): 490–501. [PubMed: 16407546]

Baumgardner TL, Reiss AL, Freund LS, Abrams MT 1995 Specification of the neurobehavioral phenotype in males with fragile X syndrome. Pediatrics. 95(5): 744–752. [PubMed: 7724315]

Berry-Kravis EM, Lindemann L, Jønch AE, Apostol G, Bear MF, Carpenter RL, Crawley JN, Curie A, Des Portes V, Hossain F and Gasparini F, 2018 Drug development for neurodevelopmental disorders: lessons learned from fragile X syndrome. Nature Reviews Drug Discovery. 17(4): 280. [PubMed: 29217836]

Bertone A, Hanck J, Kogan C, Chaudhuri A, Cornish K 2010 Associating neural alterations and genotype in autism and fragile X syndrome: Incorporating perceptual phenotypes in causal modeling. Journal of Autism and Developmental Disorders. 40(12): 1541–1548. [PubMed: 20872060]

Berzhanskaya J, Phillips MA, Shen J and Colonnese MT 2016 Sensory hypo-excitability in a rat model of fetal development in Fragile X Syndrome. Scientific reports. 6: 30769.

Berzhanskaya J, Phillips MA, Gorin A, Chongxi L, Shen J, Colonnese MT 2017 Disrupted cortical state regulation in a rat model of fragile X syndrome. Cerebral Cortex. 27(2): bbhv331.

Boone CE, Davoudi H, Harrold JB and Foster DJ, 2018 Abnormal Sleep Architecture and Hippocampal Circuit Dysfunction in a Mouse Model of Fragile X Syndrome. Neuroscience. 384: 275–289. [PubMed: 29775702]

Brock J, Brown CC, Boucher J, Rippon G 2002 The temporal binding deficit hypothesis of autism. Development and Psychopathology. 14(2): 209–224. [PubMed: 12030688]

Buzsáki G and Wang XJ, 2012 Mechanisms of gamma oscillations. Annual Review of Neuroscience. 35: 203–225.

Carrasco MM, Trujillo M and Razak KA., 2013 Development of response selectivity in the mouse auditory cortex. Hearing Research. 296: 107–120. [PubMed: 23261406]

Castrén M, Pääkkönen A, Tarkka IM, Ryynänen M, Partanen J 2003 Augmentation of auditory N1 in children with fragile X syndrome. Brain Topography. 15(3): 165–171. [PubMed: 12705812]

Chang P, Fabrizi L, Olhede S, Fitzgerald M 2016 The development of nociceptive network activity in the somatosensory cortex of freely moving rat pups. Cerebral Cortex. 1–11. [PubMed: 25139941]

Chen G, Zhang Y, Li X, Zhao X, Ye Q, Lin Y, Tao HW, Rasch MJ, Zhang X 2017 Distinct inhibitory circuits orchestrate cortical beta and gamma band oscillations. Neuron. 96(6): 1403–1418. [PubMed: 29268099]

Chen L and Toth M 2001 Fragile X mice develop sensory hyperreactivity to auditory stimuli. Neuroscience. 103(4): 1043–1050. [PubMed: 11301211]

Colonnese MT, Kaminska A, Minlebaev M, Milh M, Bloem B, Lescure S, Moriette G, Chiron C, Ben-Ari Y and Khazipov R, 2010 A conserved switch in sensory processing prepares developing neocortex for vision. Neuron. 67: 480–498. [PubMed: 20696384]

Contractor A, Klyachko VA, Portera-Cailliau C 2015 Altered neuronal and circuit excitability in fragile X syndrome. Neuron. 87(4): 699–715. [PubMed: 26291156]

Cornish K, Sudhalter V, Turk J 2004 Attention and language in fragile X. Developmental Disabilities Research Reviews, 10(1): 11–16.

Dansie LE, Phommahaxay K, Okusanya AG, Uwadia J, Huang M, Rotschafer SE, Razak KA, Ethell DW, Ethell IM 2013 Long-lasting effects of minocycline on behavior in young but not adult Fragile X mice. Neuroscience. 246: 186–198. [PubMed: 23660195]

Dasilva M, Navarro-Guzman A, Maiolo L, Ozaita A and Sanchez-Vives MV 2018 Altered Functional Connectivity in a Mouse Model of Fragile X Syndrome In: Advances in Cognitive Neurodynamics. 4: 255–261. Singapore: Springer.

Deoni SC, Dean III DC, Remer J, Dirks H O'Muircheartaigh J 2015 Cortical maturation and myelination in healthy toddlers and young children. Neuroimage. 115: 147–161. [PubMed: 25944614]

Devonshire IM, Greenspon CM, Hathway GJ 2015 Developmental alterations in noxious-evoked EEG activity recorded from rat primary somatosensory cortex. Neuroscience. 305: 343–350. [PubMed: 26254242]

Dobkin C, Rabe A, Dumas R, El Idrissi A, Haubenstock H Brown WT 2000 *Fmr1* knockout mouse has a distinctive strain-specific learning impairment. Neuroscience. 100(2): 423–429. [PubMed: 11008180]

Dölen G, Osterweil E, Rao BS, Smith GB, Auerbach BD, Chattarji S, Bear MF 2007 Correction of fragile X syndrome in mice. Neuron. 56(6): 955–962. [PubMed: 18093519]

Dvorak D and Fenton AA 2014 Toward a proper estimation of phase–amplitude coupling in neural oscillations. Journal of Neuroscience Methods. 225: 42–56. [PubMed: 24447842]

Ethridge LE, White SP, Mosconi MW, Wang J, Byerly MJ, Sweeney JA 2016 Reduced habituation of auditory evoked potentials indicate cortical hyper-excitability in fragile X syndrome. Translational Psychiatry. 6(4): e787. [PubMed: 27093069]

Frankland PW, Wang Y, Rosner B, Shimizu T, Balleine BW, Dykens EM, Ornitz EM, Silva AJ 2004 Sensorimotor gating abnormalities in young males with fragile X syndrome and *Fmr1*-knockout mice. Molecular Psychiatry. 9(4): 417. [PubMed: 14981523]

Fritz JB, David SV, Radtke-Schuller S, Yin P and Shamma SA 2010 Adaptive, behaviorally gated, persistent encoding of task-relevant auditory information in ferret frontal cortex. Nature Neuroscience. 13(8): 1011. [PubMed: 20622871]

Gibson JR, Bartley AF, Hays SA, Huber KM 2008 Imbalance of neocortical excitation and inhibition and altered UP states reflect network hyperexcitability in the mouse model of fragile X syndrome. Journal of Neurophysiology. 100(5): 2615–2626. [PubMed: 18784272]

Gogtay N, Giedd JN, Lusk L, Hayashi KM, Greenstein D, Vaituzis AC, Nugent TF, Herman DH, Clasen LS, Toga AW, Rapoport JL 2004 Dynamic mapping of human cortical development during childhood through early adulthood. PNAS. 101(21): 8174–8179. [PubMed: 15148381]

Gonçalves JT, Anstey JE, Golshani P, Portera-Cailliau C 2013 Circuit level defects in the developing neocortex of Fragile X mice. Nature Neuroscience. 16(7): 903. [PubMed: 23727819]

Gregoriou GG, Gotts SJ, Zhou H, Desimone R 2009 High-frequency, long-range coupling between prefrontal and visual cortex during attention. Science. 324(5931): 1207–1210. [PubMed: 19478185]

Hagerman RJ, Jackson AW, Levitas A, Rimland B, Braden M, Opitz JM, Reynolds JF 1986 An analysis of autism in fifty males with the fragile X syndrome. American Journal of Medical Genetics Part A. 23(1 – 2): 359–374.

Harris SW, Hessl D, Goodlin-Jones B, Ferranti J, Bacalman S, Barbato I, Tassone F, Hagerman PJ, Herman K, Hagerman RJ 2008 Autism profiles of males with fragile X syndrome. American Journal on Mental Retardation. 113(6): 427–438. [PubMed: 19127654]

Hoeft F, Carter JC, Lightbody AA, Hazlett HC, Piven J and Reiss AL, 2010 Region-specific alterations in brain development in one-to three-year-old boys with fragile X syndrome. PNAS (USA). 107: 9335–9339. [PubMed: 20439717]

Iwasa H and Potsic WP 1982 Maturational change of early, middle, and late components of the auditory evoked responses in rats. Otolaryngology--Head and Neck Surgery. 90(1): 95–102. [PubMed: 6806763]

Janusz A, Miłek J, Perycz M, Pacini L, Bagni C, Kaczmarek L, Dziembowska M 2013 The Fragile X mental retardation protein regulates matrix metalloproteinase 9 mRNA at synapses. Journal of Neuroscience. 33(46): 18234–18241. [PubMed: 24227732]

Jensen O, Kaiser J, Lachaux JP 2007 Human gamma-frequency oscillations associated with attention and memory. Trends in Neurosciences. 30(7): 317–324. [PubMed: 17499860]

Kim H, Gibboni R, Kirkhart C, Bao S 2013 Impaired critical period plasticity in primary auditory cortex of fragile X model mice. Journal of Neuroscience. 33(40): 15686–15692. [PubMed: 24089476]

Knoth IS, Vannasing P, Major P, Michaud JL, Lippé S 2014 Alterations of visual and auditory evoked potentials in fragile X syndrome. International Journal of Developmental Neuroscience. 36: 90–97. [PubMed: 24875778]

Kogan CS, Boutet I, Cornish K, Zangenehpour S, Mullen KT, Holden JJ, Der Kaloustian VM, Andermann E, Chaudhuri A 2004a Differential impact of the *FMR1* gene on visual processing in fragile X syndrome. Brain. 127(3): 591–601. [PubMed: 14736752]

Kogan CS, Bertone A, Cornish K, Boutet I, Der Kaloustian VM, Andermann E, Faubert J, Chaudhuri A 2004b Integrative cortical dysfunction and pervasive motion perception deficit in fragile X syndrome. Neurology. 63(9): 1634–1639. [PubMed: 15534248]

Kooy RF, Jin P, Bao H, Till S, Kind P, Willemsen R 2017 Chapter 7: Animal models of fragile × syndrome In: Fragile X Syndrome. 123–147. Cambridge: Academic Press.

Kuki T, Fujihara K, Miwa H, Tamamaki N, Yanagawa Y and Mushiake H, 2015 Contribution of parvalbumin and somatostatin-expressing GABAergic neurons to slow oscillations and the balance in beta-gamma oscillations across cortical layers. Frontiers in Neural Circuits. 9: 6. [PubMed: 25691859]

Lensjø KK, Christensen AC, Tennøe S, Fyhn M, Hafting T 2017 Differential expression and cell-type specificity of perineuronal nets in hippocampus, medial entorhinal cortex, and visual cortex examined in the rat and mouse. eNeuro. 4(3): ENEURO-0379.

Liu XS, Wu H, Krzisch M, Wu X, Graef J, Muffat J, Hnisz D, Li CH, Yuan B, Xu C, Li Y 2018 Rescue of fragile X syndrome neurons by DNA methylation editing of the *FMR1* gene. Cell. 172(5): 979–992. [PubMed: 29456084]

Lovelace JW, Wen TH, Reinhard S, Hsu MS, Sidhu H, Ethell IM, Binder DK, Razak KA 2016 Matrix metalloproteinase-9 deletion rescues auditory evoked potential habituation deficit in a mouse model of fragile X syndrome. Neurobiology of Disease. 89: 126–135. [PubMed: 26850918]

Lovelace JW, Ethell IM, Binder DK, Razak KA 2018 Translation-relevant EEG phenotypes in a mouse model of Fragile X Syndrome. Neurobiology of Disease. 115: 39–48. [PubMed: 29605426]

Maris E and Oostenveld R 2007 Nonparametric statistical testing of EEG-and MEG-data. Journal of Neuroscience Methods. 164(1): 177–190. [PubMed: 17517438]

Meredith RM, Dawitz J, Kramvis I 2012 Sensitive time-windows for susceptibility in neurodevelopmental disorders. Trends in Neurosciences. 35(6): 335–344. [PubMed: 22542246]

Meredith RM, 2015 Sensitive and critical periods during neurotypical and aberrant neurodevelopment: a framework for neurodevelopmental disorders. Neuroscience & Biobehavioral Reviews. 50: 180–188. [PubMed: 25496903]

Miller LJ, McIntosh DN, McGrath J, Shyu V, Lampe M, Taylor AK, Tassone F, Neitzel K, Stackhouse T, Hagerman RJ 1999 Electrodermal responses to sensory stimuli in individuals with fragile X syndrome: a preliminary report. American Journal of Medical Genetics. 83(4): 268–279. [PubMed: 10208160]

Niell CM and Stryker MP 2010 Modulation of visual responses by behavioral state in mouse visual cortex. Neuron. 65: 472–479. [PubMed: 20188652]

Nielsen DM, Derber WJ, McClellan DA, Crnic LS 2002 Alterations in the auditory startle response in *Fmr1* targeted mutant mouse models of fragile X syndrome. Brain Research. 927(1): 8–17. [PubMed: 11814427]

Nomura T, Musial TF, Marshall JJ, Zhu Y, Remmers CL, Xu J, Nicholson DA, Contractor A 2017 Delayed maturation of fast-spiking interneurons is rectified by activation of the TrkB receptor in the mouse model of fragile X syndrome. Journal of Neuroscience. 37(47): 11298–11310. [PubMed: 29038238]

O'Donnell WT and Warren ST 2002 A decade of molecular studies of fragile X syndrome. Annual Review of Neuroscience. 25(1): 315–338.

Olmos-Serrano JL, Paluszkiewicz SM, Martin BS, Kaufmann WE, Corbin JG, Huntsman MM 2010 Defective GABAergic neurotransmission and pharmacological rescue of neuronal hyperexcitability in the amygdala in a mouse model of fragile X syndrome. Journal of Neuroscience. 30(29): 9929–9938. [PubMed: 20660275]

Ponton CW, Eggermont JJ, Kwong B Don M 2000 Maturation of human central auditory system activity: evidence from multi-channel evoked potentials. Clinical Neurophysiology. 111(2): 220–236. [PubMed: 10680557]

Ponton C, Eggermont JJ, Khosla D, Kwong B, Don M 2002 Maturation of human central auditory system activity: separating auditory evoked potentials by dipole source modeling. Clinical Neurophysiology. 113(3): 407–420. [PubMed: 11897541]

Radwan B, Dvorak D and Fenton AA, 2016 Impaired cognitive discrimination and discoordination of coupled theta–gamma oscillations in *Fmr1* knockout mice. Neurobiology of Disease. 88: 125–138. [PubMed: 26792400]

Rais M, Binder DK, Razak KA and Ethell IM, 2018 Sensory Processing Phenotypes in Fragile X Syndrome. ASN neuro, 10, p.1759091418801092.

Ray S and Maunsell JH, 2011 Different origins of gamma rhythm and high gamma activity in macaque visual cortex. PLoS Biology. 9(4): e1000610. [PubMed: 21532743]

Rogers SJ, Hepburn S, Wehner E 2003 Parent reports of sensory symptoms in toddlers with autism and those with other developmental disorders. Journal of Autism and Developmental Disorders. 33(6): 631–642. [PubMed: 14714932]

Rotschafer S and Razak K 2013 Altered auditory processing in a mouse model of fragile X syndrome. Brain Research. 1506: 12–24. [PubMed: 23458504]

Rotschafer SE and Razak KA 2014 Auditory processing in fragile X syndrome. Frontiers in Cellular Neuroscience. 8: 19. [PubMed: 24550778]

Schneider A, Leigh MJ, Adams P, Nanakul R, Chechi T, Olichney J, Hagerman R, Hessl D 2013 Electrocortical changes associated with minocycline treatment in fragile X syndrome. Journal of Psychopharmacology. 27(10): 956–963. [PubMed: 23981511]

Shen J and Colonnese MT 2016 Development of activity in the mouse visual cortex. Journal of Neuroscience. 36(48): 12259–12275. [PubMed: 27903733]

Siegel JJ, Chitwood RA, Ding JM, Payne C, Taylor W, Gray R, Zemelman BV, Johnston D 2017 Prefrontal cortex dysfunction in fragile × mice depends on the continued absence of fragile x mental retardation protein in the adult brain. Journal of Neuroscience. 37(31): 7305–7317. [PubMed: 28652410]

Sinclair D, Oranje B, Razak KA, Siegel SJ, Schmid S, 2016 Sensory processing in autism spectrum disorders and Fragile X syndrome—From the clinic to animal models. Neuroscience & Biobehavioral Reviews. 76: 235–253. [PubMed: 27235081]

Sinclair D, Featherstone R, Naschek M, Nam J, Du A, Wright S, Pance K, Melnychenko O, Weger R, Akuzawa S, Matsumoto M, 2017 GABA-B agonist baclofen normalizes auditory-evoked neural oscillations and behavioral deficits in the *Fmr1* knockout mouse model of fragile X syndrome. Eneuro. 4(1): ENEURO-0380.

Sohal VS, Zhang F, Yizhar O, Deisseroth K 2009 Parvalbumin neurons and gamma rhythms enhance cortical circuit performance. Nature. 459(7247): 698. [PubMed: 19396159]

Sowell ER, Thompson PM, Holmes CJ, Jernigan TL and Toga AW, 1999 In vivo evidence for post-adolescent brain maturation in frontal and striatal regions. Nature Neuroscience. 2(10): 859. [PubMed: 10491602]

Spencer CM, Alekseyenko O, Serysheva E, Yuva-Paylor LA, Paylor R 2005 Altered anxiety-related and social behaviors in the *Fmr1* knockout mouse model of fragile X syndrome. Genes, Brain and Behavior. 4(7): 420–430.

Spencer CM, Alekseyenko O, Hamilton SM, Thomas AM, Serysheva E, Yuva - Paylor LA, Paylor R 2011 Modifying behavioral phenotypes in *Fmr1* KO mice: Genetic background differences reveal autistic-like responses. Autism Research. 4(1): 40–56. [PubMed: 21268289]

Su T, Fan HX, Jiang T, Sun WW, Den WY, Gao MM, Chen SQ, Zhao QH, Yi YH 2011 Early continuous inhibition of group 1 mGlu signaling partially rescues dendritic spine abnormalities in the *Fmr1* knockout mouse model for fragile X syndrome. Psychopharmacology. 215(2): 291–300. [PubMed: 21181121]

Van der Molen MJW, Van der Molen MW, Ridderinkhof KR, Hamel BCJ, Curfs LMG, Ramakers GJA 2012a Auditory and visual cortical activity during selective attention in fragile X syndrome: a

cascade of processing deficiencies. Clinical Neurophysiology. 123(4): 720–729. [PubMed: 21958658]

Van der Molen MJW, Van der Molen MW, Ridderinkhof KR, Hamel BCJ, Curfs LMG, Ramakers GJA 2012b Auditory change detection in fragile X syndrome males: a brain potential study. Clinical Neurophysiology. 123(7): 1309–1318. [PubMed: 22192499]

Van der Molen MJ and Van der Molen MW 2013 Reduced alpha and exaggerated theta power during the resting-state EEG in fragile X syndrome. Biological Psychology. 92(2): 216–219. [PubMed: 23182872]

Wang J, Ethridge LE, Mosconi MW, White SP, Binder DK, Pedapati EV, Erickson CA, Byerly MJ, Sweeney JA, 2017 A resting EEG study of neocortical hyperexcitability and altered functional connectivity in fragile X syndrome. Journal of Neurodevelopmental Disorders. 9(1): 11. [PubMed: 28316753]

Wen TH, Afroz S, Reinhard SM, Palacios AR, Tapia K, Binder DK, Razak KA, Ethell IM 2017 Genetic reduction of matrix metalloproteinase-9 promotes formation of perineuronal nets around parvalbumin-expressing interneurons and normalizes auditory cortex responses in developing *Fmr1* knock-out mice. Cerebral Cortex. 13: 1–14.

Winkowski DE, Nagode DA, Donaldson KJ, Yin P, Shamma SA, Fritz JB and Kanold PO 2017 Orbitofrontal cortex neurons respond to sound and activate primary auditory cortex neurons. Cerebral Cortex. 28(3): 868–879.

Yan QJ, Asafo - Adjei PK, Arnold HM, Brown RE Bauchwitz RP 2004 A phenotypic and molecular characterization of the *Fmr1* - tm1Cgr Fragile X mouse. Genes, Brain and Behavior. 3(6): 337–359.

Yu S, Pritchard M, Kremer E, Lynch M, Nancarrow J, Baker E, Holman K, Mulley JC, Warren ST, Schlessinger D, Sutherland GR 1991 Fragile X genotype characterized by an unstable region of DNA. Science. 1179–1181. [PubMed: 2031189]

Zhang Y, Bonnan A, Bony G, Ferezou I, Pietropaolo S, Ginger M, Sans N, Rossier J, Oostra B, LeMasson G, Frick A 2014 Dendritic channelopathies contribute to neocortical and sensory hyperexcitability in *Fmr1*−/y mice. Nature Neuroscience. 17(12): 1701. [PubMed: 25383903]

Highlights:

- Development of EEG phenotypes in *Fmr1* KO mice were examined
- Baseline gamma power was increased in the frontal cortex at all ages tested
- N1 amplitude and gamma power of ERP was increased in *Fmr1* KO mice at P21
- Data reveal EEG/ERP deficits in frontal and auditory cortex in early development

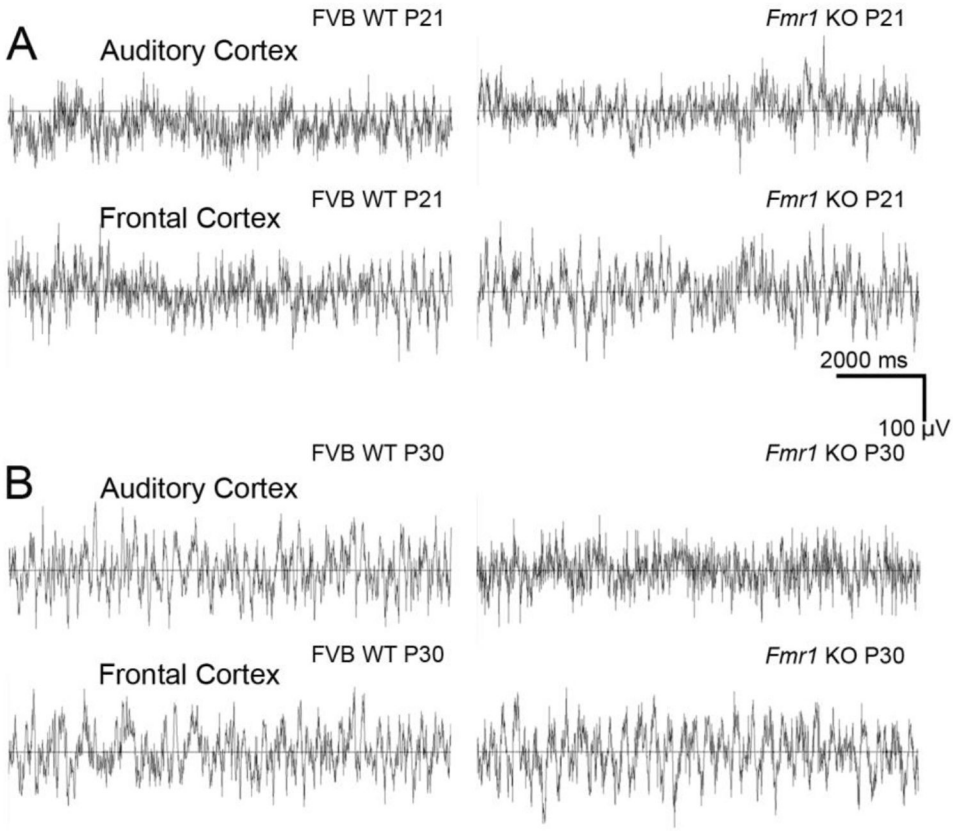

Figure 1. EEG traces recorded from WT and Fmr1 KO auditory and frontal cortex.

(A) Example raw EEG waveforms recorded from WT (left) and KO (right) auditory and frontal cortex at P21. ***(B)*** Example raw EEG waveforms recorded from WT (left) and KO (right) auditory and frontal cortex at P30.

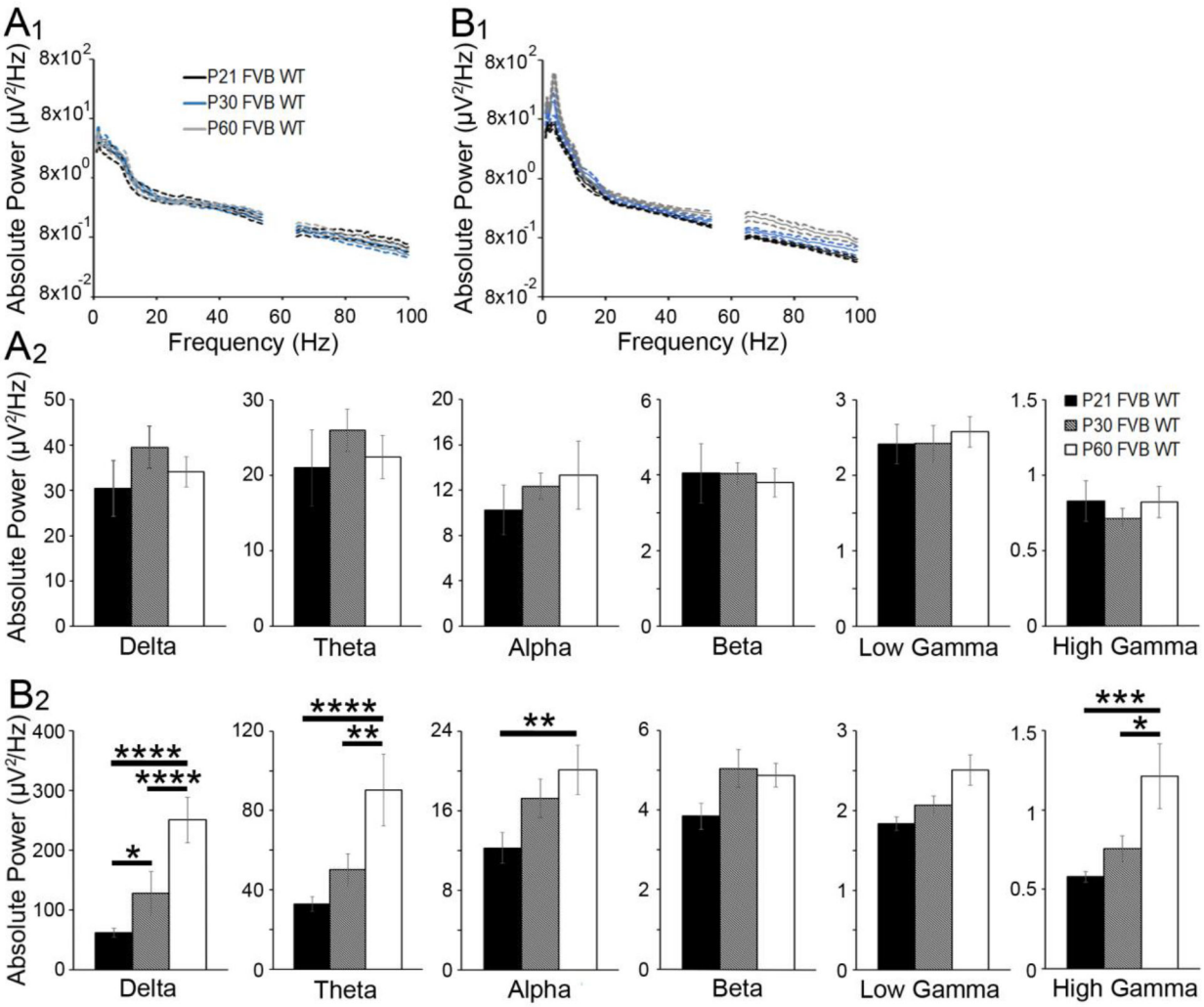

Figure 2. Developmental changes in absolute spectral power of EEG in WT cortex.

(A1) Average absolute power (± SEM, dashed lines) in WT auditory cortex at P21 (black), P30 (blue), and P60 (gray) as a function of frequency. ***(A2)*** Average absolute power in delta, theta, alpha, beta, low gamma, and high gamma frequency bands, respectively (mean ± SEM). Average absolute power increased from P21 to P30 in WT auditory cortex. ***(B1)*** Average absolute power (± SEM, dashed lines) in WT frontal cortex at P21 (black), P30 (blue), and P60 (gray) as a function of frequency. ***(B2)*** In WT frontal cortex, average absolute power increased with age. Note the ordinate range is different for panels A2 and B2.

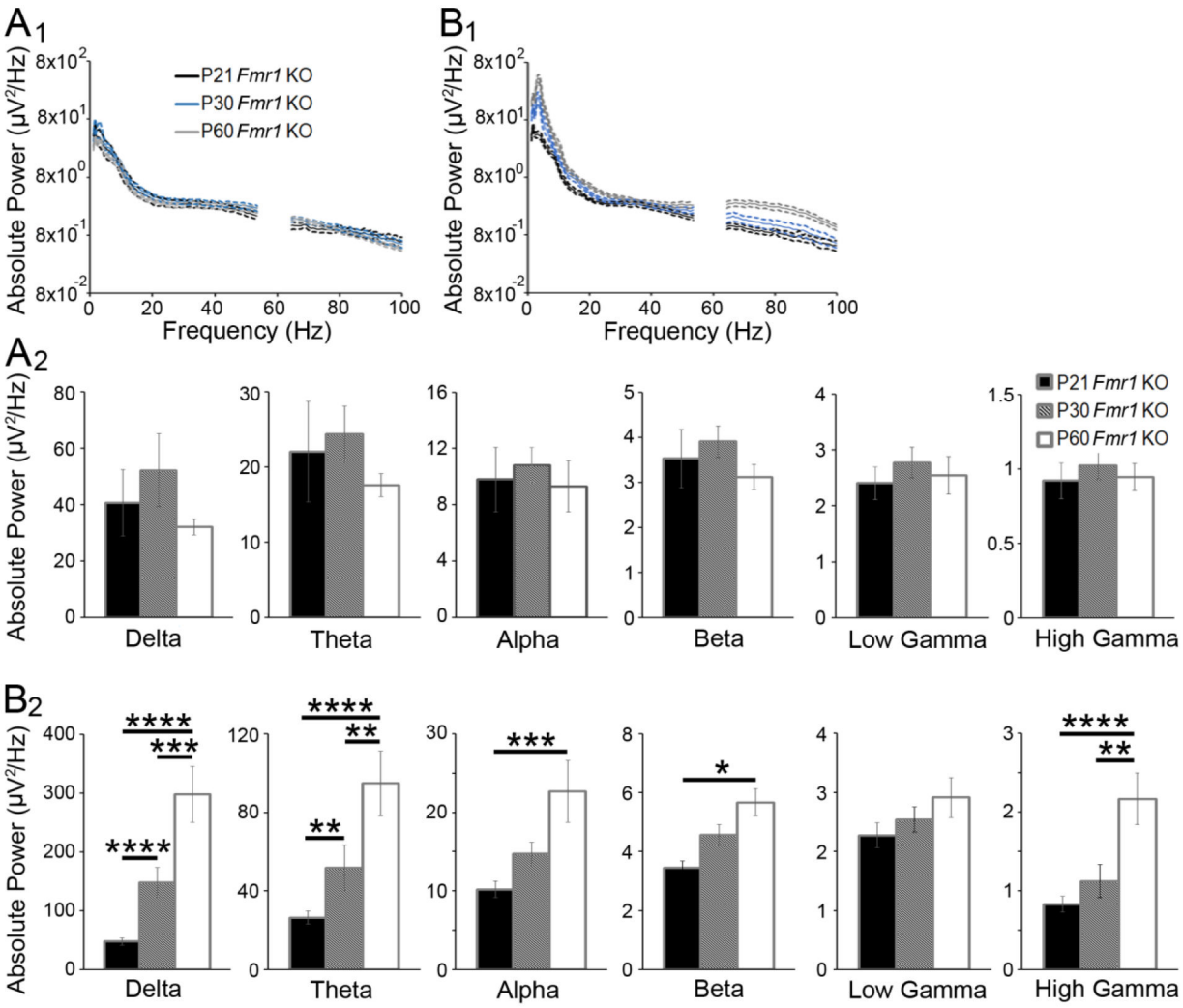

Figure 3. Developmental changes in absolute spectral power in Fmr1 KO cortex.

(A1) Average absolute power (± SEM, dashed lines) in *Fmr1* KO auditory cortex at P21 (black), P30 (blue), and P60 (gray) as a function of frequency. **(A2)** Average absolute power in delta, theta, alpha, beta, low gamma, and high gamma frequency bands, respectively (mean ± SEM). Average absolute power increased from P21 to P30 in KO auditory cortex. **(B1)** Average absolute power (± SEM, dashed lines) in KO frontal cortex at P21 (black), P30 (blue), and P60 (gray) as a function of frequency. **(B2)** Average absolute power in frontal cortex increased with age. Note the ordinate range is different for panels A2 and B2.

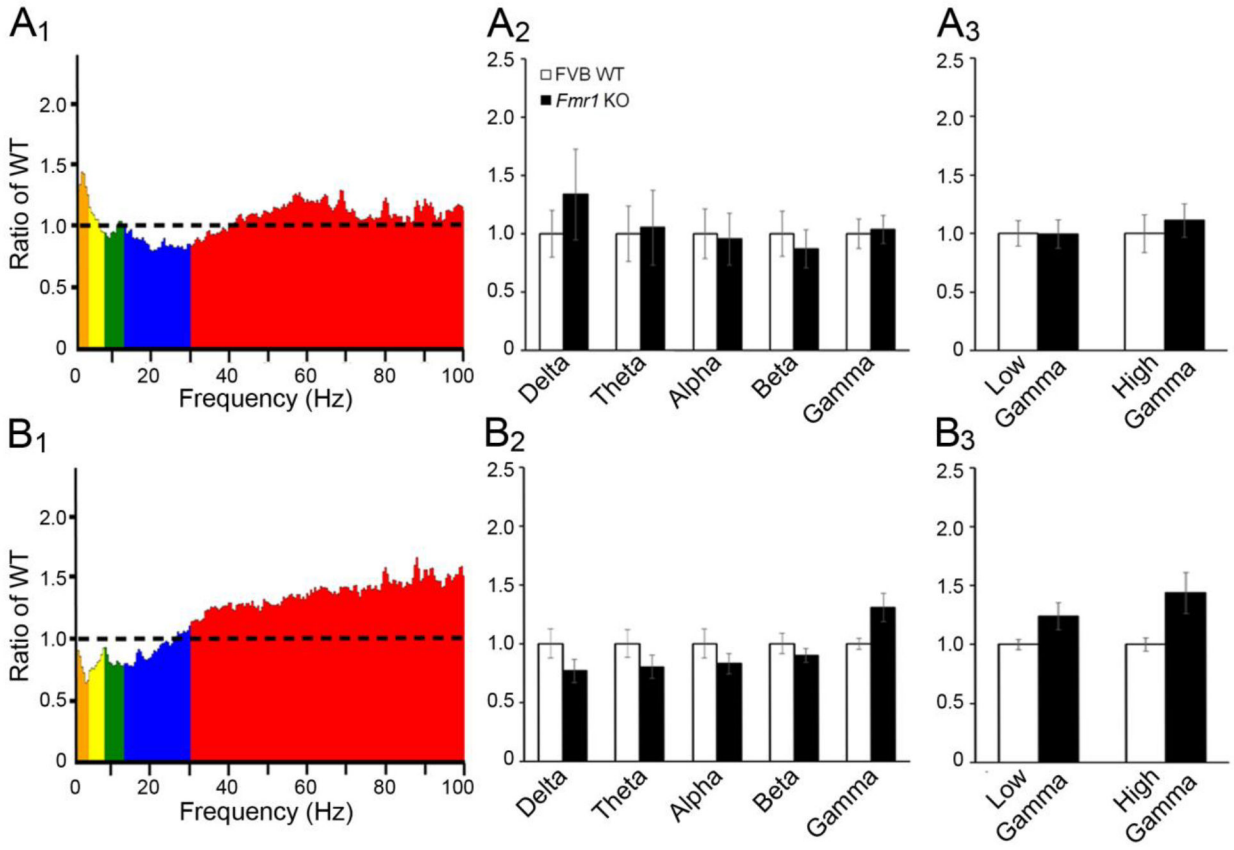

Figure 4. Comparison of EEG power between WT and Fmr1 KO cortex at P21 shows enhanced gamma power in frontal cortex.

(A1) Average absolute EEG power in P21 *Fmr1* KO auditory cortex divided by the average absolute power in P21 WT auditory cortex. The ordinate is the ratio between KO and WT power with value = 1 indicating identical power and values >1 indicating more power in the KO mouse. **(A2)** Normalized power in auditory cortex across all frequency bands. Power across all frequency bands in *Fmr1* KO auditory cortex was comparable to WT. **(A3)** Absolute power in low and high gamma frequency bands was comparable in WT and *Fmr1* KO auditory cortex. **(B1)** Absolute EEG power in P21 *Fmr1* KO frontal cortex normalized to average absolute power in P21 WT frontal cortex. **(B2)** In frontal cortex, power across all frequency bands in *Fmr1* KO frontal cortex was comparable to WT. **(B3)** When gamma band power was divided into low (30–54 Hz) and high (64–100 Hz) frequency bands, an increase in gamma power was observed in the *Fmr1* KO mouse compared to WT.

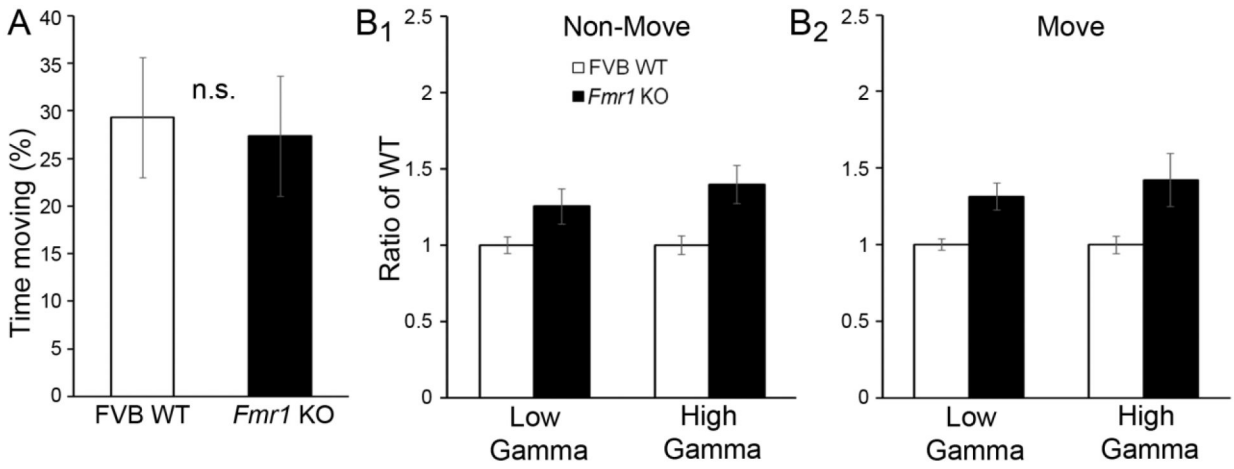

Figure 5. Enhanced gamma in FC at P21 was independent of mouse movement.

(A) Movement of the mouse was sensed using a piezoelectric crystal placed under the cage. The percentage of time spent moving was not significantly different between WT and *Fmr1* KO mice. **(B)** EEG recordings were separated between 'non-move' ***(B1)*** and 'move' ***(B2)*** according to movement state. Power was higher in low and high gamma frequency bands in *Fmr1* KO FC independent of movement state.

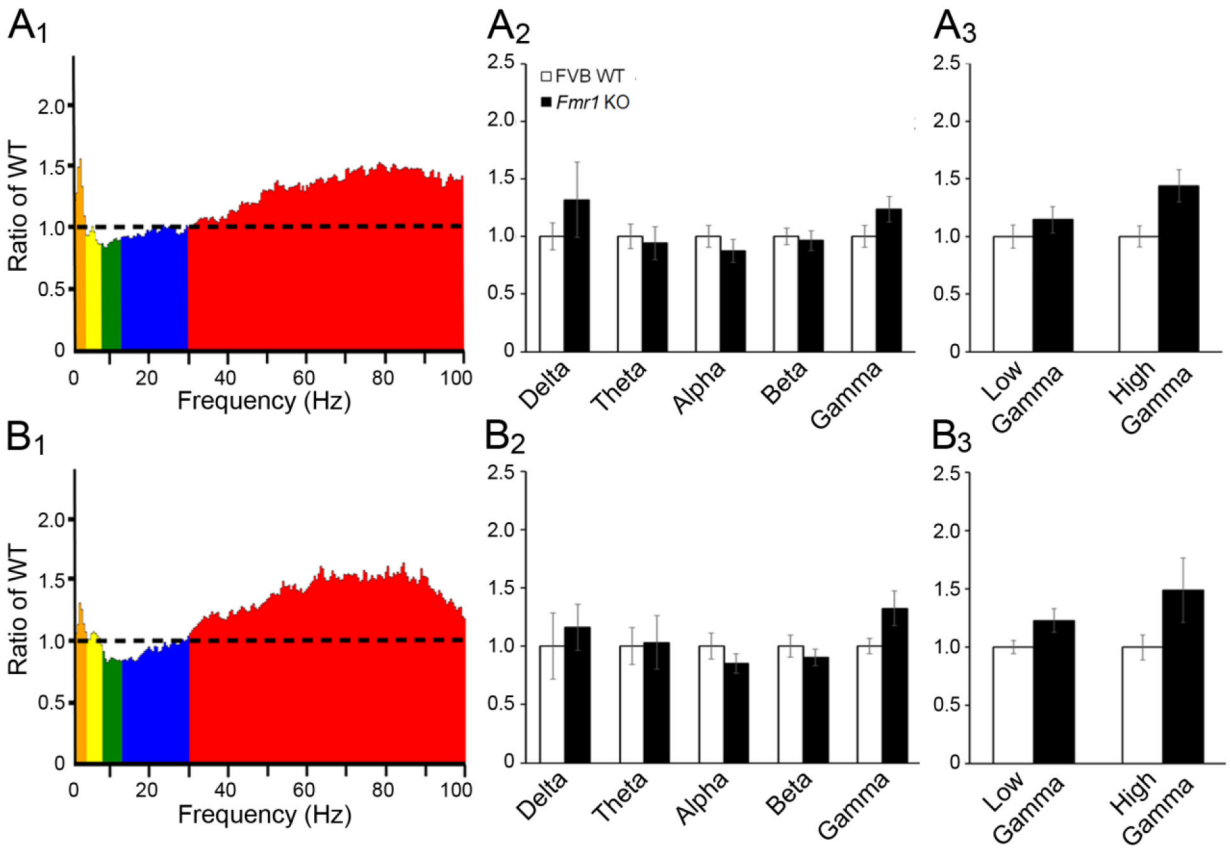

Figure 6. Enhanced gamma power in Fmr1 KO mice was seen at P30 in both auditory and frontal cortex.

(A1) Absolute EEG power in P30 *Fmr1* KO auditory cortex normalized to average absolute power in WT auditory cortex. **(A2)** Normalized power in P30 auditory cortex across all frequency bands was comparable between WT and *Fmr1* KO. **(A3)** When gamma band power was separated into low gamma and high gamma frequency bands, there was increased gamma in both high and low frequency bands. **(B1)** Absolute EEG power in P30 WT *Fmr1* KO frontal cortex normalized to average absolute power in WT frontal cortex. **(B2)** Normalized power in P30 frontal cortex across all frequency bands was comparable between WT and *Fmr1* KO. **(B3)** When gamma band power was separated into low gamma and high gamma frequency bands, there was increased gamma in both high and low frequency bands.

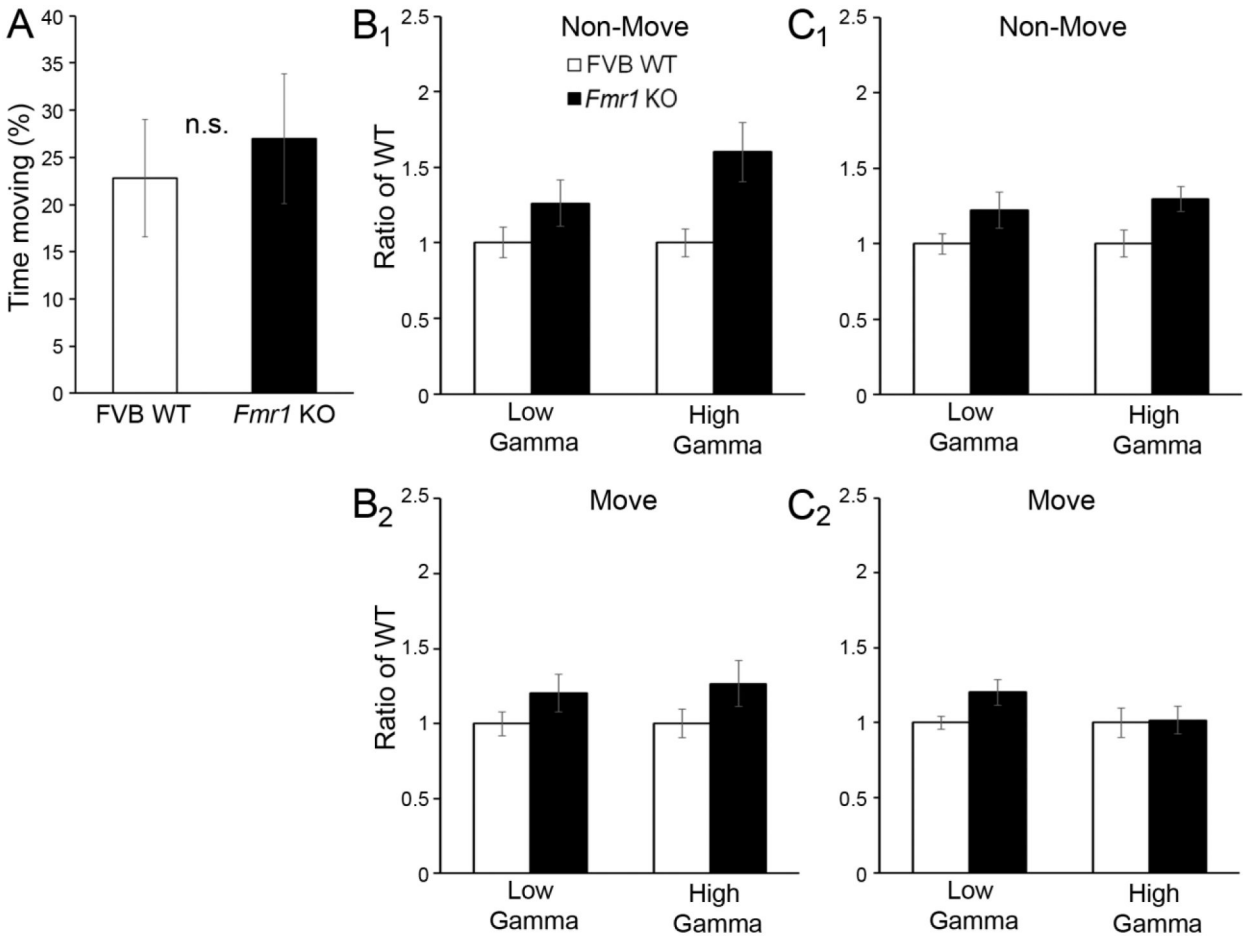

Figure 7. Enhanced gamma in both auditory and frontal cortex at P30 was independent of mouse movement.

(A) The percentage of time spent moving was not significantly different between WT and *Fmr1* KO mice. **(B1, B2)** Power was increased in low and high gamma frequency bands in *Fmr1* KO auditory cortex independent of movement state. **(C1, C2)** Power was increased in low and high gamma frequency bands in *Fmr1* KO frontal cortex independent of movement state.

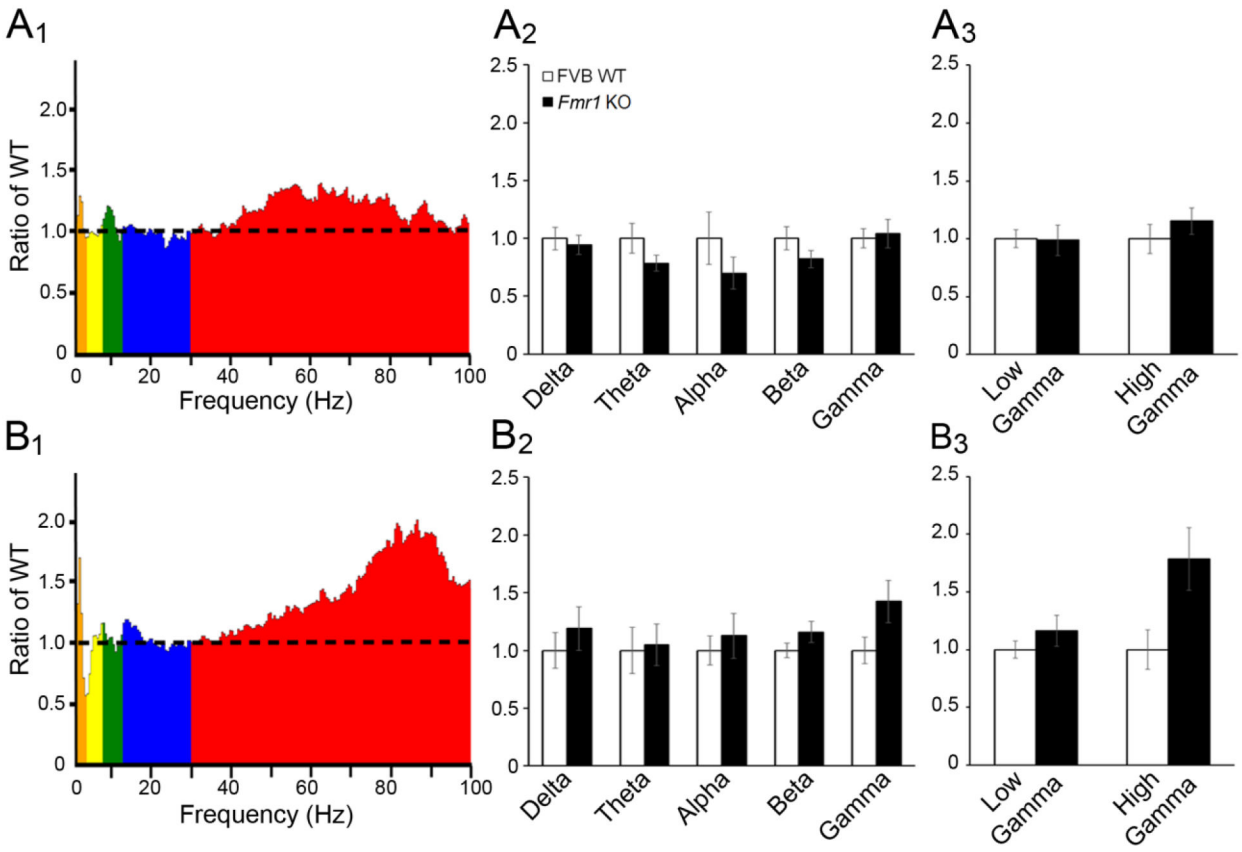

Figure 8. Comparison of EEG power between adult WT and Fmr1 KO cortex shows enhanced gamma power in the frontal cortex.

(A1) Absolute EEG power in *Fmr1* KO auditory cortex normalized to average absolute power in WT auditory cortex. ***(A2)*** Normalized power in P30 auditory cortex across all frequency bands was comparable between WT and *Fmr1* KO. ***(A3)*** Power in low and high gamma frequency bands was comparable between WT and *Fmr1* KO auditory cortex. ***(B1)*** Absolute EEG power in *Fmr1* KO frontal cortex normalized to average absolute power in WT frontal cortex. ***(B2)*** Normalized power in frontal cortex was not different between WT and *Fmr1* KO. ***(B3)*** When gamma was divided into low and high gamma frequency bands, there was increased gamma power in *Fmr1* KO frontal cortex.

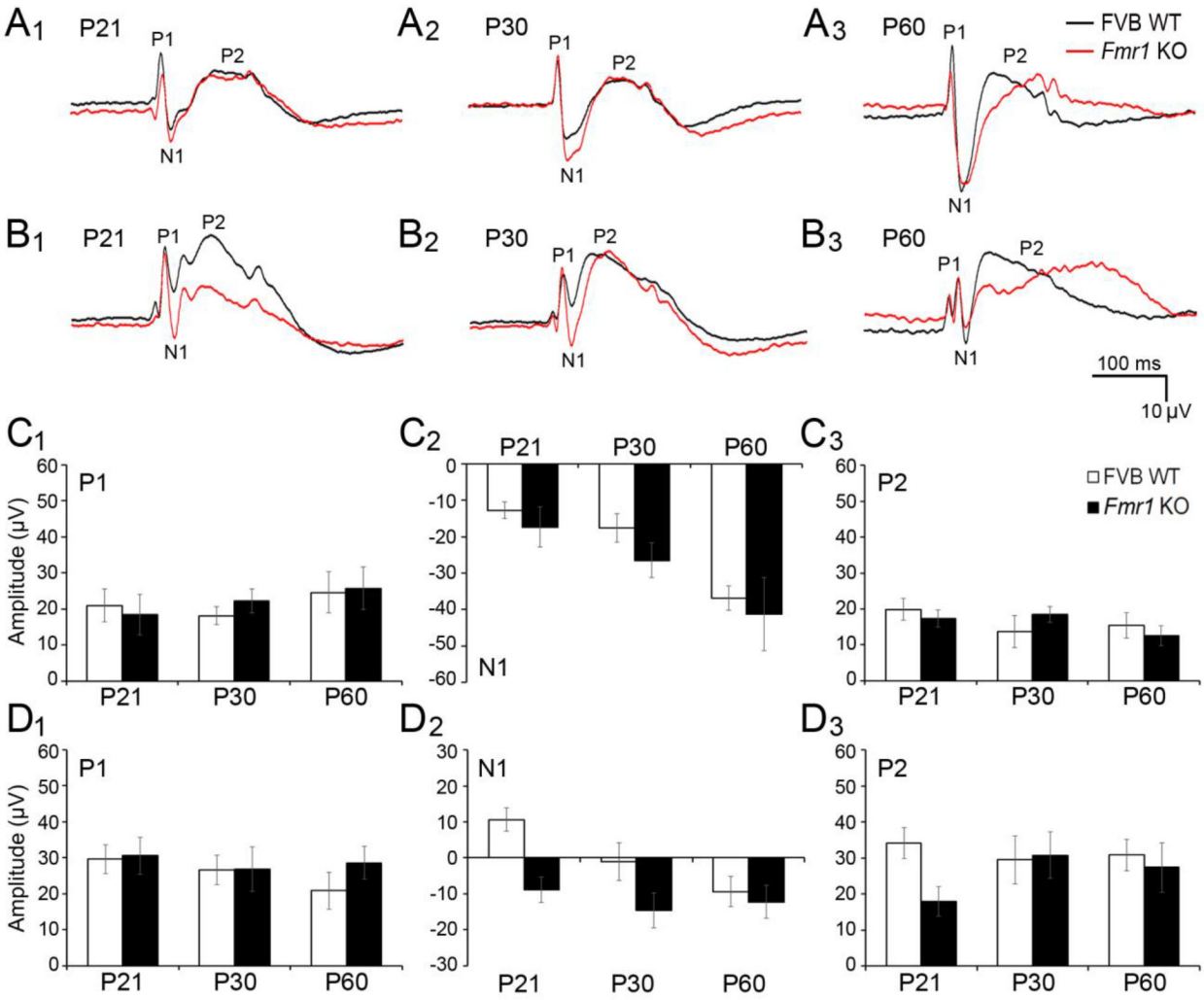

Figure 9. Development of auditory ERPs in auditory and frontal cortex of WT and Fmr1 KO mice.

(A-B) Grand average ERPs obtained from P21, P30, and P60 WT (black) and *Fmr1* KO (red) mouse auditory cortex ***(A1, A2, A3)*** and frontal cortex ***(B1, B2, B3)*** in response to 100 ms broadband noise presented at 0.25 Hz repetition rate. P1, N1, and P2 were defined as maximum or minimum voltage deflections within 0–30 ms, 30–80 ms, or 80–150 ms, respectively. ***(C-D)*** Quantification of ERP amplitudes in auditory ***(C1, C2, C3)*** and frontal ***(D1, D2, D3)*** cortex of WT (white) and *Fmr1* KO (black) mice. There was a developmental increase in N1 amplitude in auditory cortex ***(C2)***. Larger N1 amplitudes were seen in frontal cortex of *Fmr1* KO mice ***(D2)***. Age- and genotype-related differences were not observed for P1 ***(C1, D1)*** and P2 ***(C3, D3)***.

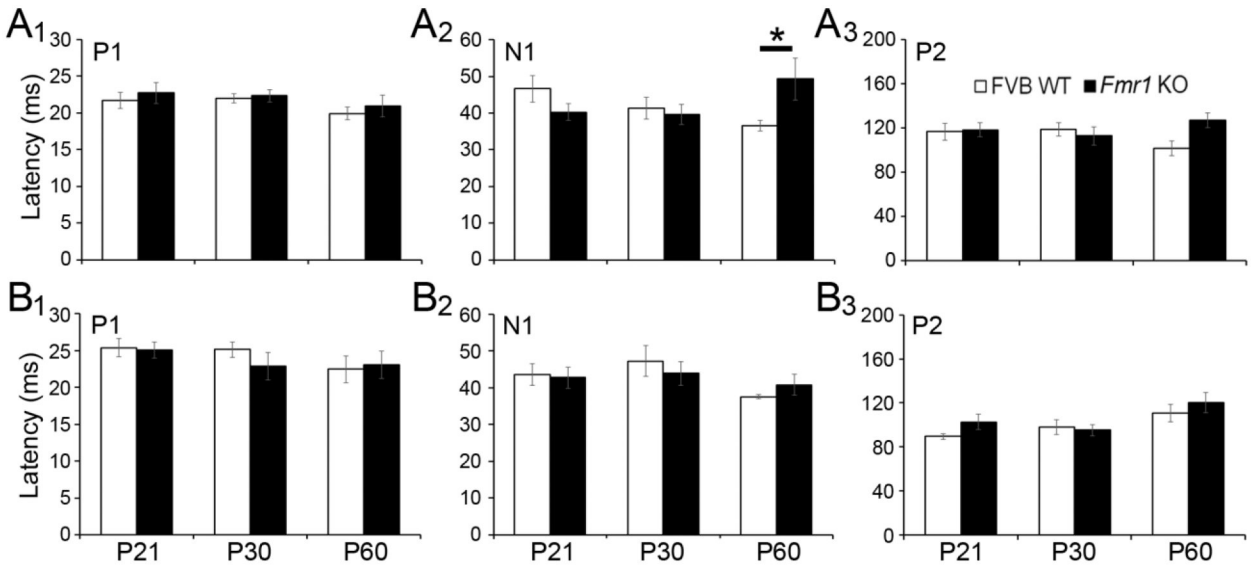

Figure 10. Developmental and genotype differences in auditory ERP latencies.

P1 ***(A1)***, N1 ***(A2)***, and P2 ***(A3)*** latencies from ERP waveforms evoked in in WT (white) and *Fmr1* KO (black) auditory cortex. There was an age-related decrease in N1 latency in frontal cortex in both WT and *Fmr1* KO mice. N1 latency was increased in adult *Fmr1* KO auditory cortex. P1 and P2 latencies were not different across development or genotype. P1 ***(B1)***, N1 ***(B2)***, and P2 ***(B3)*** latencies from ERP waveforms evoked in in WT (white) and *Fmr1* KO (black) frontal cortex.

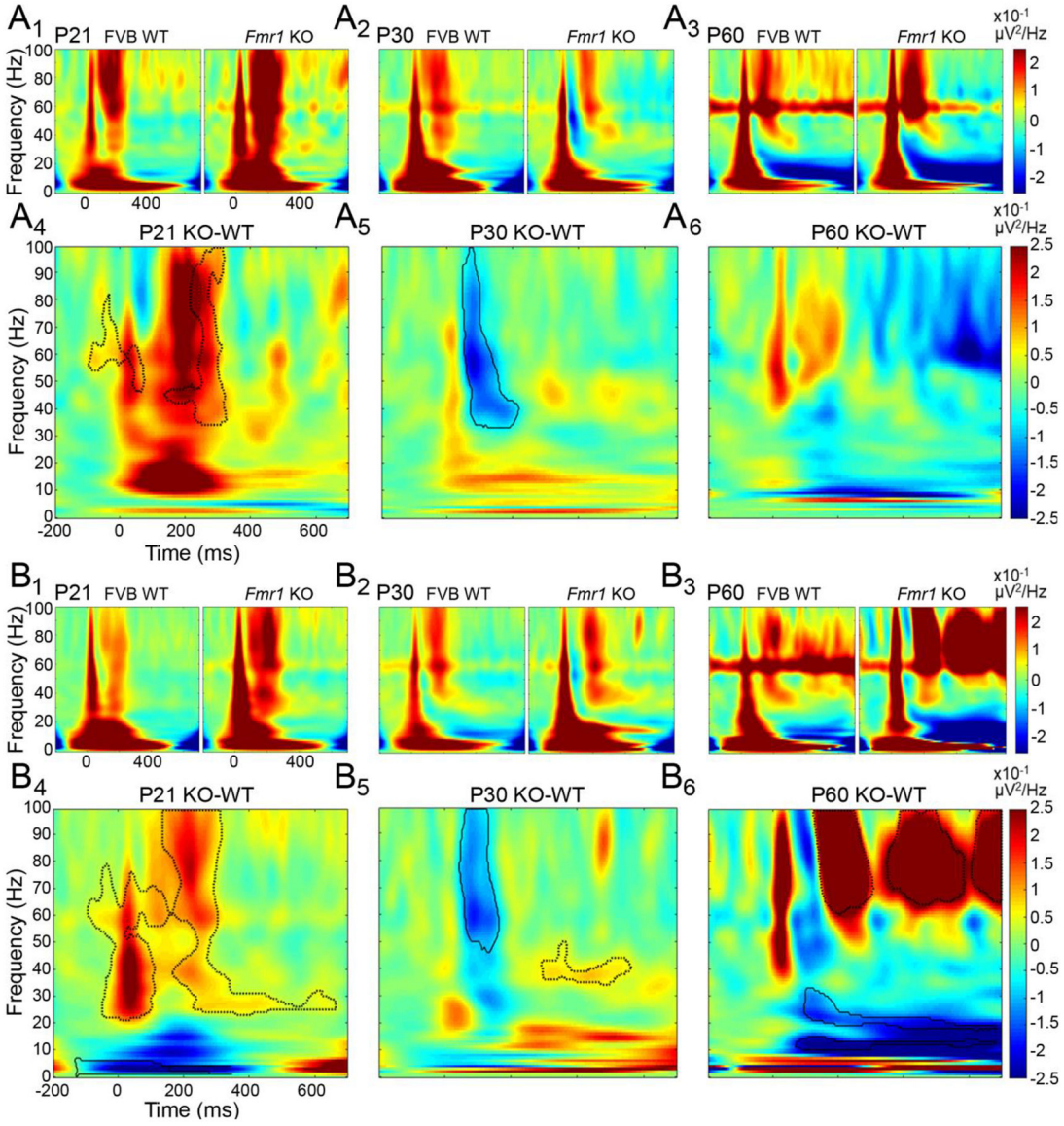

Figure 11. Non-phase locked gamma power in ERP is altered in developing and adult Fmr1 KO mice.

WT and KO differences in non-phase locked gamma power in AC ***(A)*** and FC ***(B)***. Warmer colors indicate increased power in KO compared to WT. Cooler colors indicate reduced power in KO compared to WT. In P21 AC ***(A1, A4)*** and FC ***(B1, B4)*** of KO mice, non-phase locked power was significantly increased in the gamma frequency range. At P30, both KO AC ***(A2, A5)*** and KO FC ***(B2, B5)*** exhibited reduced non-phase locked power in the gamma frequency range. At P60, non-phase locked power in the gamma frequency range was increased in KO FC ***(B3, B6)***. Black contours indicate clusters which are significant different between WT and KO.

Table 1.
Summary of strain-specific changes in EEG/ERP measures in adults.

Developmental studies have not been conducted in Fmr1 KO mice on the C57/Bl6 background.

MOUSE STRAIN	Age	*Fmr1* KO AC	*Fmr1* KO FC
C57/Bl6	P21–24	**?**	**?**
C57/Bl6	P28–34	**?**	**?**
C57/Bl6	Adult	↑ baseline gamma	↑ baseline gamma ↑ N1 amplitude
FVB	P21–24	↑ non-phase locked gamma	↑ baseline gamma ↑ N1 amplitude ↑ non-phase locked gamma
FVB	P28–34	↑ baseline gamma ↓ non-phase locked gamma	↑ baseline gamma ↑ N1 amplitude ↓ non-phase locked gamma
FVB	Adult	↑ N1 latency	↑ baseline gamma ↑ N1 amplitude ↑ ongoing non-phase locked gamma